

# Don't Let Gains FADE: Breaking Down Policy Gradient Weights in RL

Juliette Decugis<sup>1,2</sup>, Sean O'Brien\*, Francis Bach<sup>2</sup>, Gabriel Synnaeve<sup>1</sup>, Taco Cohen<sup>1</sup>

<sup>1</sup>FAIR at Meta, <sup>2</sup>Inria, Ecole Normale Supérieure

\*Work done at Meta, now working at the University of California, San Diego

Reinforcement learning post-training dramatically improves LLM reasoning, but suffers from training instability and diversity collapse. Advantage functions offer an appealing fix: they reshape the training objective, reweight which rollouts drive learning, and are trivial to implement. Yet a proliferation of methods makes it unclear which advantage to use and when. We cut through the confusion with a unifying framework that decomposes any advantage into its positive and negative gradient mass ( $m_S$ ,  $m_F$ ) along two orthogonal axes. On the sign axis, imbalanced updates collapse either entropy or weight geometry. On the difficulty axis, hard-problem focus sharpens signal but costs sample size. Both trade-offs shift during training: exploration favors balance and hard focus; exploitation favors suppression and medium focus. This motivates FADE (Focal Advantage with Dynamic Entropy), a self-adapting advantage that reads training dynamics to schedule the gradient weight automatically. FADE reaches peak pass@1 20k steps earlier than the best static baseline at the 7B scale and 2k steps earlier at the 32B, while achieving the best accuracy-diversity trade-off across all pass@ $k$  on LiveCodeBench and AIME.

**Date:** July 3, 2026

**Correspondence:** Juliette Decugis at [jdecugis@meta.com](mailto:jdecugis@meta.com)



## 1 Introduction

Recent developments in reinforcement learning with verifiable rewards (RLVR) have unlocked rapid gains in language models' capabilities, especially in easily-verifiable domains like code generation and mathematics (OpenAI, 2024; Guo et al., 2025; Shao et al., 2024; Liu et al., 2025a). Although sparse rewards over long sequences make credit assignment challenging (Minsky, 1961; Sutton, 1988; Zhang, 2026), pretrained LLMs provide strong behavioral priors (Gan and Isola, 2026; Yan et al., 2025) and fully resettable environments enable parallel rollout collection. These methods therefore follow a common recipe: sample multiple rollouts per problem, score them with a binary verifier, and update the policy via a weighted policy gradient (Williams, 1992; Schulman et al., 2015). The weights, commonly called "advantage functions," rarely correspond to the classical advantage (value of an action minus the value of the average action in a state); they simply determine how much each rollout contributes to the gradient. To avoid this overloading, we use the term *policy weights* throughout this paper.

Since GRPO (Shao et al., 2024), which uses the mean reward as a baseline for updates, a host of alternative policy weights have appeared: DAPO (Yu et al., 2025), DR-GRPO (Liu et al., 2025a), pass@ $k$ -based objectives (Tang et al., 2025; Chen et al., 2025), log-mean-exp weighting (Jiang et al., 2025), and more. Each claims improvements, yet comparing them is difficult because they differ along multiple axes simultaneously. Consider for example the pass@8 normalization (Tang et al., 2025), which only upweights a correct rollout when it is the sole success in a batch of eight. This simultaneously shifts gradient mass toward hard problems, drops all negative gradient signal since incorrect rollouts receive zero weight, and reduces the overall gradient magnitude because most batches contain either zero or more than one success. Other methods such as Skew-R (Thrampoulidis et al., 2025) keep the sign balance of GRPO  $\mathbb{E}[A] = 0$  but emphasize high variance samples. When these methods under or outperform GRPO, it is unclear which change is responsible.

We argue that the confusion stems from conflating three orthogonal design axes. Similar to Thrampoulidis et al. (2025), we decompose policy weights into positive  $m_S$  and negative  $m_F$  mass on the gradient (Section 2)

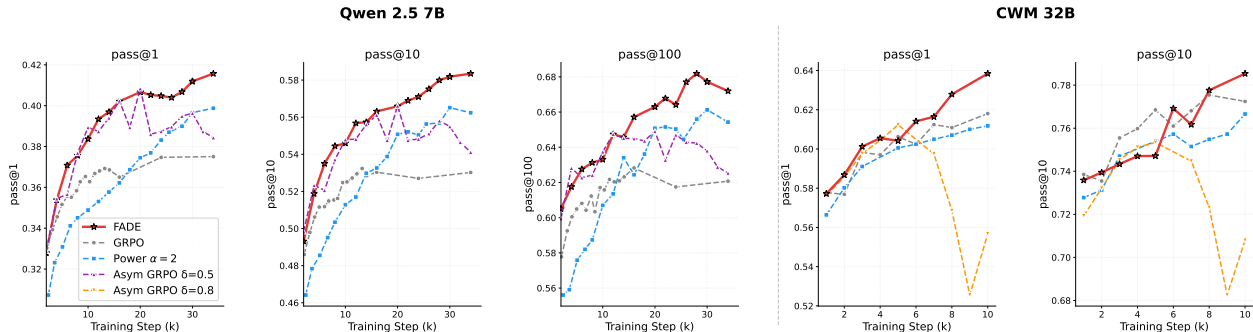


**Figure 1** FADE learns faster and better for all pass@k on LiveCodeBench v6 when compared to GRPO and the best static advantages power  $\alpha$  and Asymmetric GRPO with the best  $\delta$  per model.

which are dependent on a prompt’s solve rate  $p$ . We show policy weights can differ along:

1. **Difficulty Axis:** whether gradient mass peaks on easy prompts (high  $p$ ) or hard ones (low  $p$ );
2. **Sign Axis:** whether the positive and negative masses are equal or not;
3. **Scale Axis:** the overall magnitude of the gradient, which implicitly rescales the learning rate.

We identify three trade-offs driven by the representational asymmetry between correct and incorrect trajectories:

- **Reinforcing successes collapses entropy.** Because correct solutions cluster tightly, amplifying them concentrates the policy onto a narrow mode, with the drift rate predictable from the sign ratio alone (Section 4.1).
- **Suppressing failures induces rank-1 update collapse.** Because failures are diverse and decorrelated, amplifying them drives the weight update toward a single suppression direction, progressively blocking multi-dimensional learning (Section 4.2).
- **Harder problems trade information for variance.** Focusing gradient mass on low-solve-rate prompts yields more informative updates, but at the cost of more variance (Section 4.3).

Since a fixed advantage cannot adapt to all three trade-offs during training, we propose **FADE** (Focal Advantage with Dynamic Entropy) which shapes its gradient weight based on the policy’s past entropies and solve rates. It achieves fast early learning with sustained diversity and accuracy across model scales (7B, 32B) (Section 5).

## 2 Framework for Policy Weight Analysis

We view the LLM as a policy  $\pi_\theta$  that generates a trajectory of tokens  $\tau := (a_1, \dots, a_T)$  given a prompt  $q$  with  $\log \pi_\theta(\tau) = \sum_{t=0}^T \log \pi_\theta(a_t | q, a_{<t})$ . In LLM post-training, the reward  $r(\tau)$  is typically a single scalar assigned at the end of the trajectory (e.g., correctness of the final answer) which we maximize using the policy gradient estimator (Williams, 1992):  $\mathbb{E}_{\tau \sim \pi_\theta} [r(\tau)] = \mathbb{E}_{\tau \sim \pi_\theta} [r(\tau) \nabla_\theta \log \pi_\theta(\tau)]$ .

Compared to supervised learning, the model learns from its own generations reweighted by a verifier which can introduce noise. To reduce variance (Schulman et al., 2015), the reward is replaced by a weight function  $W(\tau)$ , originally the advantage  $A(s_t, a_t) = Q(s_t, a_t) - V(s_t)$  (Baird, 1993), and more recently a variety of alternatives based on the average solve rate per problem (Table 1). We will show that balancing between positive and negative gradient mass is the key to stable, efficient and diverse RL at scale.

### 2.1 Positive and Negative Gradient Mass

We will assume that rewards are binary, with  $r(\tau) \in \{0, 1\}$ , and that the policy weight is a function of success/failure only. In this setting, we can consider the set of successful and unsuccessful trajectories  $S = r^{-1}(1)$  and  $F = r^{-1}(0)$ . Since  $r$  is deterministic and binary-valued, the joint distribution  $\mathbb{P}(r = 1, \tau) =$

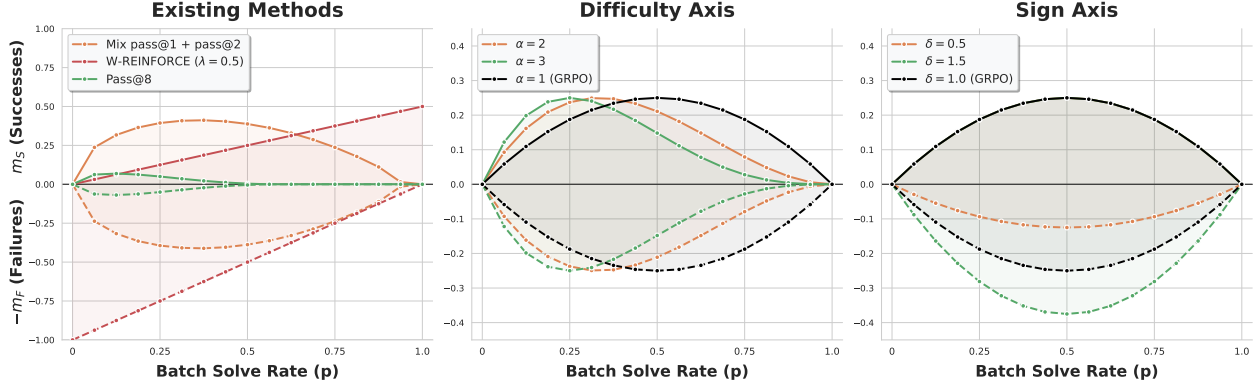


**Figure 2 Effect of Policy Weights on Batch Level Gradients** based on the estimated solve rate  $p$ . **(Left)** Existing methods: mixing pass@ $k$  [Chen et al. \(2025\)](#) and W-REINFORCE [Zhu et al. \(2025\)](#) modify the sign, difficulty focus and scale of advantages. We design weights that isolate **(Middle)** the difficulty axis with the Power  $\alpha$  series  $p(1-p)^\alpha$  and **(Right)** sign axis with the AsymGRPO series where  $\frac{p(1-p)}{\delta}$  for failed trajectories.

$\mathbb{P}(r = 1|\tau)\pi_\theta(\tau) = \mathbb{I}[\tau \in S]\pi_\theta(\tau)$ , and similarly for  $r = 0$ . Hence the probability of success is given by  $p = \sum_{\tau \in S} \pi_\theta(\tau)$ , and failure  $q = 1 - p = \sum_{\tau \in F} \pi_\theta(\tau)$  and we write the policy weight as:

$$W(\tau) = w_S \cdot \mathbb{I}[\tau \in S] - w_F \cdot \mathbb{I}[\tau \in F]. \quad (1)$$

Adapting the notation from previous work ([Thrapoulidis et al., 2025](#)), we can write the policy gradient as

$$\nabla_\theta J = w_S \cdot p \cdot \mathbb{E}[\nabla_\theta \log \pi_\theta(\tau) \mid \tau \in S] - w_F \cdot q \cdot \mathbb{E}[\nabla_\theta \log \pi_\theta(\tau) \mid \tau \in F]. \quad (2)$$

In practice, when doing online reinforcement learning we don't have access to the true solve rate  $p$  but estimate via  $G$  Monte Carlo rollouts from our policy  $\pi_\theta$ :

$$\nabla_\theta J \approx \underbrace{w_S \cdot \bar{p}}_{\bar{m}_S} \underbrace{\frac{1}{|\bar{S}|} \sum_{\tau \in \bar{S}} \nabla_\theta \log \pi_\theta(\tau)}_{\bar{\nabla}_S} - \underbrace{w_F \cdot \bar{q}}_{\bar{m}_F} \underbrace{\frac{1}{|\bar{F}|} \sum_{\tau \in \bar{F}} \nabla_\theta \log \pi_\theta(\tau)}_{\bar{\nabla}_F}, \quad (3)$$

where  $\bar{S}$  and  $\bar{F}$  are the positive and negative trajectories in  $G$ ,  $\bar{p} = |\bar{S}|/|G|$  and  $\bar{q} = |\bar{F}|/|G|$  are the empirical estimates of the success and failure probability, respectively. Here  $\bar{\nabla}_S$ ,  $\bar{\nabla}_F$  are the average log-probability gradients over successful and failed trajectories in the batch. For notational convenience, we will often leave out the bar when discussing estimates when it can be inferred from context.

## 2.2 GRPO as an Example

Consider a group of  $G$  rollouts per prompt, we take as policy weight the reward minus the mean (mean only GRPO by GRPO ([Liu et al., 2025a](#))). With  $r \in \{0, 1\}$ , we have  $\mathbb{E}[A] = \bar{p}$  and successful trajectories receive  $A_s = 1 - \bar{p}$ , failed ones  $A_f = 0 - \bar{p}$ , yielding

$$\begin{aligned} \nabla_{\text{GRPO}} &= \sum_{\tau \in \bar{S}} A_s \nabla \log \pi_\theta(\tau) + \sum_{\tau \in \bar{F}} A_f \nabla \log \pi_\theta(\tau) \\ &= (1-p) \sum_{\tau \in \bar{S}} \nabla \log \pi_\theta(\tau) - p \sum_{\tau \in \bar{F}} \nabla \log \pi_\theta(\tau) \end{aligned} \quad (4)$$

$$\begin{aligned} &= |\bar{S}|(1-p) \underbrace{\frac{1}{|\bar{S}|} \sum_{\tau \in \bar{S}} \nabla \log \pi_\theta(\tau)}_{\bar{\nabla}_S} - |\bar{F}|p \underbrace{\frac{1}{|\bar{F}|} \sum_{\tau \in \bar{F}} \nabla \log \pi_\theta(\tau)}_{\bar{\nabla}_F} \\ &\approx Gp(1-p) \bar{\nabla}_S - G(1-p)p \bar{\nabla}_F \end{aligned} \quad (5)$$

$$= Gp(1-p)[\bar{\nabla}_S - \bar{\nabla}_F]. \quad (6)$$

Mean based GRPO reweights gradients by the estimated variance of rewards (Suk and Duan, 2025). It focuses on medium difficulty problems since  $\arg \max_p p(1-p) = \frac{1}{2}$  (Figure 2). Similarly many recent policy weights depend only on the average solve rate per batch so we can define their positive and negative mass as functions of  $\bar{p}$  (see examples in Table 1, complete derivations in Appendix A). We distinguish sign-balanced advantages ( $m_S = m_F$ ) and sign-biased methods ( $m_S \neq m_F$ ).

**Table 1 Weight functions as positive  $m_S$  vs. negative mass  $m_F$**  on our policy gradients where our final update consists of  $m_S \cdot \bar{\nabla}_S - m_F \cdot \bar{\nabla}_F$ . We assume binary rewards for successful vs. failed trajectories and use  $r_i \in \{0, 1\}$  for simplicity (one can generalize to other ranges with a multiplier) so  $\mathbb{E}[r] = \hat{p}$ . Notation: expected number of correct  $p$  and incorrect  $q := 1 - p$  samples per batch.

Method	Weight $W(\tau)$	$m_S$	$m_F$
<b>Sign-balanced (<math>m_S = m_F</math>)</b>			
GRPO (Shao et al., 2024)	$\frac{r_i - \bar{p}}{\sigma_R}$		$\sqrt{pq}$
Dr. GRPO (Liu et al., 2025a)	$r_i - \bar{p}$		$pq$
RLOO (Ahmadian et al., 2024)	$r_i - \frac{1}{G-1} \sum_{j \neq i} r_j$		$\frac{G}{G-1} pq$
Skew-R (Thrampoulidis et al., 2025; Kimi Team et al., 2025)	$(r_i - \bar{p}) \frac{r_i - \bar{p}}{\sigma_R}$		$pq \sqrt{pq}$
Binary Contrastive (Greensmith et al., 2004)	$[\mathbf{1}_{r=1} - \frac{\bar{p}}{1-\bar{p}} \mathbf{1}_{r=0}]$		$p$
Power Norm (Andrychowicz et al., 2021)	$\frac{r_i - \bar{p}}{[\bar{p}(1-\bar{p})]^\gamma}$		$p^{1-\gamma} q^{1-\gamma}$
Softmax (Shao et al., 2024)	$\text{softmax}_\beta(r) - \frac{1}{G}$		$\frac{(e^\beta - 1)pq}{1 + p(e^\beta - 1)}$
MaxRL (Tajwar et al., 2026)	$\frac{r_i - \bar{p}}{\bar{p}}$		$q$
Analytical pass@k (Chen et al., 2025)	$\frac{q^{k-1}(r_i - \bar{p})}{\sigma_k}$		$p \sqrt{\frac{q^k}{1-q^k}}$
Mix pass@1/pass@k (Chen et al., 2025)	$p \hat{A}_{pass@k} + q \hat{A}_{pass@1}$	$p$	$q$
F-GRPO (Plyusov et al., 2026)	$(1-p)^\alpha \frac{r_i - \bar{p}}{\sigma_R}$	$(1-p)^\gamma$	$\sqrt{p(1-p)}$
T2T (Lin et al., 2026)	$\frac{(r_i - \bar{p})(1 - \alpha p \bar{L}_S - \alpha q \bar{L}_F)}{\sigma_R}$		$\sqrt{pq}(1 - \alpha p \bar{L}_S - \alpha q \bar{L}_F)$
Power $\alpha$ (ours)	$(r_i - \bar{p}) q^{\alpha-1}$		$p q^\alpha$
Positive Power $\alpha$ (ours)	$(r_i - \bar{p}) \cdot \bar{p}^{1+\lceil r < \bar{p} \rceil} \cdot (1 - \bar{p})^\alpha$		$p^\alpha q$
<b>Sign-biased (<math>m_S \neq m_F</math>)</b>			
REINFORCE (Sutton et al., 1999)	$r_i$	$p$	$q$
Constant Baseline (Sutton et al., 1999)	$r_i - C$	$(1-C)p$	$Cq$
Symmetric clip (Schulman et al., 2017)	$\text{clip}(r_i - \bar{p}, -c, c)$	$p \min(c, q)$	$q \min(c, p)$
W-REINFORCE (Zhu et al., 2025)	$\min(\lambda r, r)$	$\lambda p$	$q$
Pass@k (Tang et al., 2025)	$\max_k(r) - \max_k(r_{-i})$	$k p q^{k-1}$	$0$
Quantile baseline (Dabney et al., 2018)	$r_i - \mathbf{1}_{\tau > q}$	$p \mathbf{1}_{\tau \leq q}$	$q \mathbf{1}_{\tau > q}$
Logmeanexp (Jiang et al., 2025)	$\text{lme}_\beta(r) - \text{lme}_\beta(r_{-i})$	$\frac{p e^\beta}{p e^\beta + q}$	$\frac{q}{p e^\beta + q}$
MC-GRPO (Kim, 2026)	$r_i - \text{med}(r)$	$p \mathbf{1}[p \leq \frac{1}{2}]$	$q \mathbf{1}[p > \frac{1}{2}]$
CoRPO (Garg and Venkatesh, 2025)	$r_i - \max(r_{\min}, \bar{p})$	$p(1-r_{\min})$	$q r_{\min}$
AsymRL (Arnal et al., 2026)	$r_i - (\bar{p} + \delta)$	$p(q - \delta)$	$q(p + \delta)$
HA-DW (Yang et al., 2026)	$A \cdot \lambda \exp(-\text{sgn}(\hat{A}) \text{sgn}(\hat{r} - C_t)  \hat{r} - C_t )$	$f(C_t, p) pq$	$qp$
ReLU (Srinivasan et al., 2018)	$\max(0, r_i - \bar{p})$	$pq$	$0$
Asym. power $\alpha$ (ours)	$(r - \bar{p})[\mathbf{1}_{r \geq \bar{p}} q^{\alpha_s - 1} + \mathbf{1}_{r < \bar{p}} p^{\alpha_n - 1}]$	$p q^{\alpha_s}$	$p^{\alpha_n} q$
Asym. GRPO (ours)	$(r - \bar{p})[\mathbf{1}_{r \geq \bar{p} + \frac{1}{\delta}} + \frac{1}{\delta} \mathbf{1}_{r < \bar{p}}]$	$pq$	$\frac{pq}{\delta}$

### 3 Experimental Setup

The framework above shows that each advantage function induces a different balance of positive and negative gradient mass, but it does not predict which balance leads to the best policies. To answer this, we compare advantage functions along different weight axes within the PPO clipping framework (Schulman et al., 2017) using two model sizes: the Qwen 2.5 7B (Hui et al., 2024), and the Code World Model 32B SFT checkpoint (FAIR CodeGen team et al., 2025) (CWM 32B). All evaluations use temperature 1.0 and top-p 1.0 to promote sampling diversity, at reasoning budgets from 8k to 30k tokens.

**Reasoning SFT.** The Qwen 2.5 7B model lacks chain-of-thought capability, so we first fine-tune it on a mix of reasoning chains including OpenCodeReasoning-2 (Ahmad et al., 2025) and OpenMathReasoning (Moshkov et al., 2025) generated by DeepSeek-R1 (Guo et al., 2025) using the same <think> tags formatting. CWM 32B is already trained to produce long chain-of-thought responses so we skip the supervised fine-tuning (SFT).

**RL training.** We train with binary rewards (format and answer correctness) on 25,000 competitive programming problems including the CodeContest (Li et al., 2022) and TACO (Li et al., 2023) training sets. The dataset is fixed throughout training and epoched over: for Qwen 2.5 7B we use the full problem mix (initial solve rate  $\approx 0.3$ ), while for CWM 32B we filter out easy problems to start at a similar difficulty frontier ( $\approx 0.5$  solve rate). In this work we do not modify the training data distribution and instead focus on maximizing gradient learning through the policy weight given a fixed dataset. See Appendix D.1 for infrastructure details.

Starting from the same SFT checkpoint, we train models with different advantage functions and analyze policies along four complementary axes: accuracy (pass@1 (Chen et al., 2021)), diversity (pass@100), reasoning generalization on AIME 2024/2025 math competitions (OpenAI, 2024) a task unseen during RL training, and learning speed. Full results across all methods, models, and benchmarks are in Tables 4 and 5 in Appendix D.2.

## 4 Where to learn from? Balancing gradient signs and problem difficulty

Should we focus on reinforcing successes or suppressing failures within a batch? And on easy, medium, or hard problems across batches? During online RL, we are simultaneously doing gradient descent to downweight failed trajectories and gradient ascent to upweight successful trajectories. We analyze how to balance reinforcing successes (Section 4.1), suppressing failures (Section 4.2), and adjusting the focus per difficulty (Section 4.3) to reach +14% pass@1 in  $2\times$  less training steps over the default reward weight (REINFORCE Sutton (1988)).

### 4.1 Reinforcing Successes Collapses Entropy

#### Takeaway

Entropy collapse is proportional to the sign ratio and success rates  $\Rightarrow$  Bias toward successes only at low solve rates.

We introduce **AsymGRPO**, a single-parameter variant of GRPO that keeps the same positive mass  $m_S = p(1-p)$  and rescales the negative mass by  $\delta$ ,  $m_F = \frac{p(1-p)}{\delta}$ . With this  $\delta$  knob we can either amplify or downweight failures; with  $\delta = 1$  we recover standard mean based GRPO. Because correct solutions are few and similar, amplifying them ( $\delta > 1$ ) rapidly concentrates the policy onto a narrow set of actions. Adapting the analysis of Cui et al. (2025) (Appendix F), a first-order Taylor expansion of the entropy after a gradient step with learning rate  $\eta$  is:

$$\Delta \mathcal{H} \approx \eta \left[ \underbrace{(m_S - m_F) \mathcal{H}}_{\text{entropy drift}} - \text{Cov}(A, \log \pi_\theta) \right] + O(\eta^2). \quad (7)$$

The covariance term drives entropy loss for all methods it is the standard mechanism studied in prior work (Cui et al., 2025). The drift term, however, is unique to sign-imbalanced advantages where  $m_S \neq m_F$  and introduces entropy-proportional feedback. Under AsymGRPO this feedback is controlled entirely by  $\delta$ :

- $\delta = 1$ : drift is zero, entropy collapses through the covariance term alone, with no mechanism to recover.
- $\delta > 1$ : drift is positive ( $m_S > m_F$ ), accelerating collapse beyond what the covariance predicts. Entropy loss feeds into itself since the drift is proportional to  $\mathcal{H}$ .
- $\delta < 1$ : drift is negative ( $m_S < m_F$ ), providing a restoring force that slows entropy loss.

Empirically we find entropy correlates tightly with the advantage ratio  $\frac{A_s}{A_f} := \frac{m_S \times p}{m_F \times q}$  (Figure 4) so it can be steered by changing the training data (adjusting average solve rates  $p$ ) or by rebalancing gradient mass

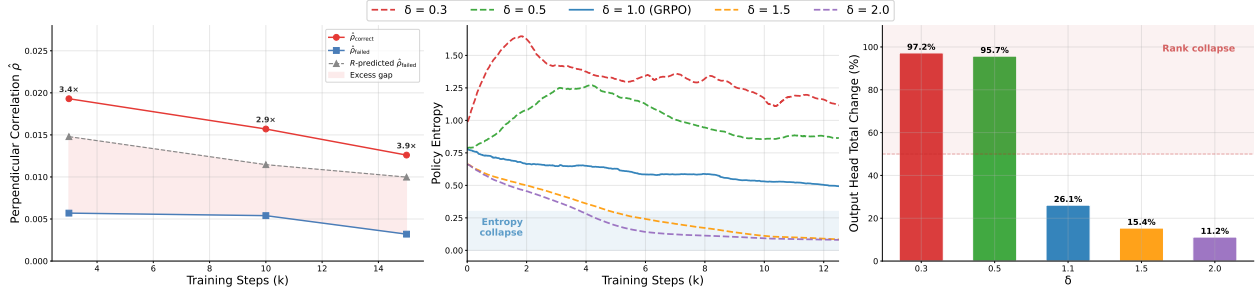


**Figure 3** Scaling negative gradients of mean GRPO ( $\delta < 1$ : up,  $\delta > 1$ : down) on Qwen 2.5 7B. **(Left)** For AsymGRPO with  $\delta = 0.5$ , correct samples are far more correlated than failures, whose pairwise residual correlation  $\rho_{\perp}$  is  $2\times$  below the value predicted by the higher-rank residual  $R = \mathbb{E}[A_i v_i \otimes h_i^{\perp}]$  (Appendix H). **(Middle)** Over-reinforcing ( $\delta > 1$ ) causes entropy collapse; **(Right)** over-suppressing ( $\delta < 1$ ) causes rank-1 update collapse.

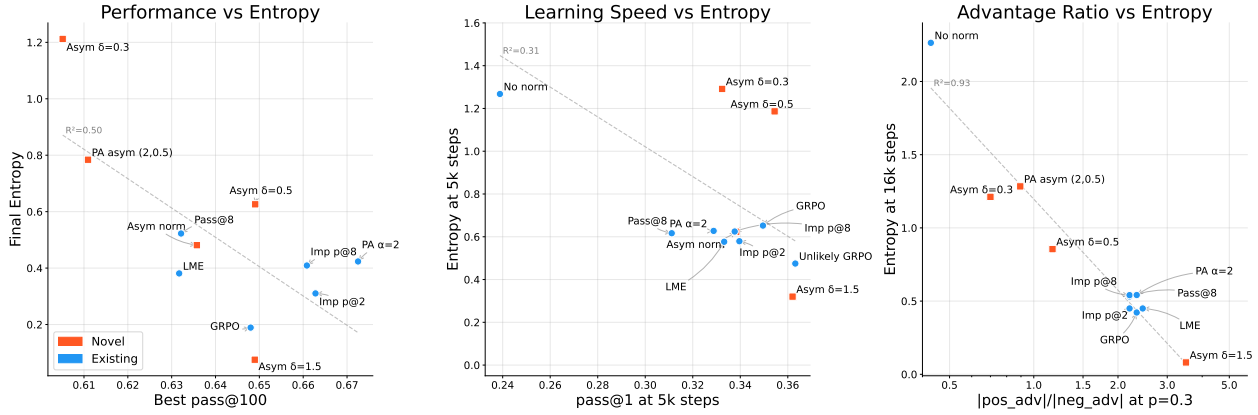


**Figure 4** The policy’s entropy is not correlated with pass@100 or learning speed; instead, it is proportional to the advantage sign:  $m_S \cdot p / m_F \cdot (1 - p)$  with  $m_S$ ,  $m_F$  the mass of successful and failed trajectories respectively,  $p$  our solve rate.

between reinforcing and suppressing ( $m_S$  vs.  $m_F$ ). Since LLMs are prone to entropy collapse in online RL (Park et al., 2025; Khatri et al., 2025),  $\delta < 1$  delays overfitting and accelerates exploration at the start of training (Figure 3). However, as we show next, pushing  $\delta$  too far below 1 trades one pathology for another.

## 4.2 Suppressing failures induces rank-1 update collapse

### Takeaway

Failure bias learns fast but collapses the update to rank-1.  $\Rightarrow$  Reserve failure bias for late-stage exploitation.

Failure-biased methods (our own AsymGRPO with  $\delta < 1$ , Asymmetric Power  $\alpha$  and existing methods such as AsymNorm Arnal et al. (2026)) maintain high entropy and show fast early reward and pass@1. Yet the gains are fragile: reward eventually degrades, answer diversity (pass@100) drops, and GRPO catches up (Tables 4 and 5). What makes learning from failures unreliable?

Analyzing the weight change  $W_{\Delta} = W_{\text{rl}} - W_{\text{sft}}$  throughout training (Appendix H), we find that all methods start rank-1 dominant in the output weight change (using SVD analysis on  $W_{\Delta}$ ). Sign-balanced and success-biased methods gradually escape (Figure 5), while failure-biased methods ( $\delta < 1$ ) remain locked in rank-1, with RL change concentrating almost entirely in the output head (up to 90% of  $\|W_{\Delta}\|_2$  at 7B, Table 9, Figure 3). We call this the *rank-1 funnel*: it enables fast early exploitation but progressively blocks further learning as the model can only update along one axis, ultimately reducing diversity (pass@100) and out-of-distribution generalization on AIME 2024/2025 (Tables 4 and 5).

What causes this rank-1 funnel? We formalize this by decomposing the output-head of the RL change  $W_\Delta$  gradient into a rank-1 signal and a higher-rank residual (see details in Appendix H.1):

$$W_\Delta = \sum_{i=1}^N A_i v_i \otimes h_i = \underbrace{\left( \sum_{i=1}^N A_i \alpha_i v_i \right)}_{M_1 \text{ (rank 1)}} \otimes u_1 + \underbrace{\sum_{i=1}^N A_i v_i \otimes h_i^\perp}_{M_2 \text{ (higher rank)}}. \quad (8)$$

We measure collapse via  $r_1 = \frac{\sigma_1^2(W_\Delta)}{\|W_\Delta\|_F^2}$ : the fraction of the update’s energy in its leading singular direction, which arises from two conditions:

1. **Per-step:** We project each hidden state  $h_i$  onto the leading shared direction  $u_1$  and measure how correlated the residuals  $h_i^\perp = h_i - (h_i^\top u_1) u_1$  are across samples. The average pairwise correlation of these residuals,  $\rho_\perp$ , controls the higher-rank term  $M_2$ : when  $\rho_\perp \rightarrow 0$  the residuals are mutually uncorrelated and their weighted sum cancels out, so  $M_2$  vanishes and  $r_1 \rightarrow 1$  (Appendix H.1). Empirically, failure hidden states are far more diverse than correct ones ( $\rho_{\perp, \text{fail}} \ll \rho_{\perp, \text{correct}}$ , Appendix H): summing over many uncorrelated failure residuals leaves only the shared “suppress non-code tokens” direction  $u_1$ . Setting  $\delta < 1$  amplifies this noisy failure mass while downweighting the correlated successes, pushing  $M_2$  toward zero and  $r_1$  toward 1 (Figure 3).
2. **Across steps:** if each per-step gradient aligns in the same direction, the accumulated  $W_\Delta$  is itself rank-1. Empirically, cosine similarity between successive batch gradients converges to  $\approx 1$  from step 600 on for negatively biased methods, turning per-step dominance into cumulative collapse. In contrast, sign-balanced methods have lower alignment or switch rank-1 direction (Appendix H.3).

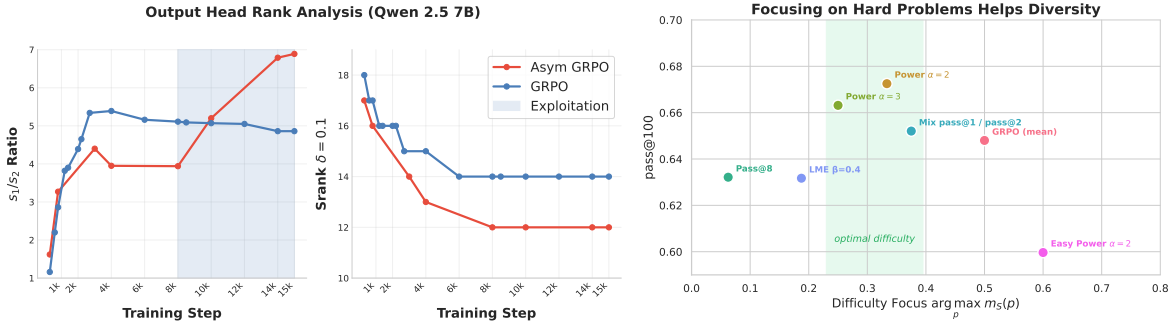


**Figure 5 (Left)** Failure-biased methods converge to a lower-rank weight update than sign-balanced methods as shown by the singular-value ratio  $s_1/s_2$  of the output head of  $W_\Delta = W_{sft} - W_{rl}$ , and its  $\text{rank}_\delta = \min\{k : \sum_{i=1}^k s_i / \sum_{i=1}^d s_i \geq 1 - \delta\}$  (Kumar et al., 2020). **(Right)** Pass@100 on LCB v6 as a function of the difficulty focus in policy weights.

### 4.3 Harder problems trade information for variance

#### Takeaway

Hard problems yield more informative gradients but fewer usable batches  $\Rightarrow$  Focus on hard problems early, relax toward medium difficulty as solve rates rise.

We showed biasing batch updates towards reinforcing or suppressing trajectories can lead to overexploitation either in the policy or weight space. For now, we only reweighted successes and failures based on the weight sign, but in practice some batches deserve more gradient attention than others. For example, our policy should explore new ways of reasoning to solve harder problems rather than overfit to the easy ones. Approximating the  $k$  vs.  $\text{pass}@k$  curve as  $\text{pass}@k = \exp(-a(k+c)^{-b})$  (Brown et al., 2024; Schaeffer et al., 2025, see also Appendix E), we also notice the difficulty axis is relevant to preserve diversity. All methods lose scaling slope  $b$  during training except  $\text{pass}@k$ -driven weights (evaluations done on LCB v6, Figure 6, Figure 13), which also achieve the highest final  $\text{pass}@100$  for competitive programming and math at both model scales (Table 3, 5). To understand how this difficulty axis shapes learning, we introduce **Power**  $\alpha$ :  $m_S = m_F = C \cdot pq^\alpha$  ( $C$

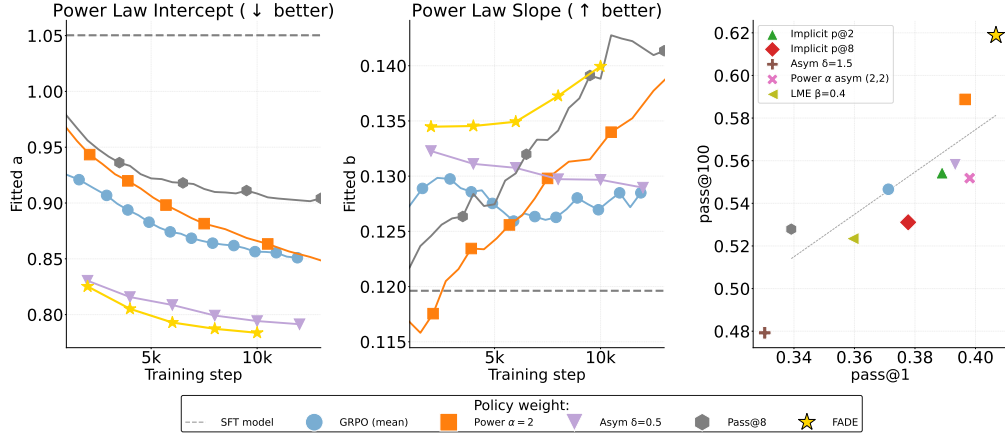


**Figure 6 Accuracy vs. Diversity per Policy Weight** We estimate the  $k$  vs.  $\text{pass}@k$  curve by a shifted power law  $G(k) = \exp(-a(k+c)^{-b})$  where  $a$  controls the uniform level and  $b$  controls the steepness. **(Left)** Evolution during training of these coefficients where diverse RL should increase  $b$  or at least maintain  $b$  and lower  $a$ . **(Right)**  $\text{pass}@100$  vs.  $\text{pass}@1$  where diverse accurate advantages maximize both.

normalizes the peak to match the GRPO scale), a smooth approximation of  $\text{pass}@k$  advantages (Chen et al., 2025) (Figure 2) inspired by the focal loss of Lin et al. (2017). Higher  $\alpha$  biases the gradient towards harder problems. Its easy counterpart uses  $C \cdot p^\alpha q$ .

Sweeping  $\alpha$  values, we find focusing on solve rates  $\hat{p} \in [0.3, 0.5]$  (Figure 5) maximizes both  $\text{pass}@1$  and  $\text{pass}@100$ . We analyze why this optimal difficulty exists. Across batches, the most valuable gradients at a solve rate  $p$  are the ones with high signal  $s(p)$ , low variance  $\text{Var}(w(\hat{p})\hat{g})$ , and high frequency. Since we estimate the empirical success rate  $\bar{p}$  via  $G$  Monte Carlo rollouts, the variance of the weight  $\bar{w} = w(\hat{p})$  is a random variable. Using the Delta method, we can estimate the total per-update noise as:

$$\text{Var}(w(\hat{p})\hat{g}) \approx w(p)^2 v_0(p) + s(p)^2 \text{Var}(w(\hat{p})) \quad (9)$$

where  $v_0(p) \propto \frac{1}{G p(1-p)}$  is the raw gradient variance (which blows up when successes or failures are rare see Figure 7), and  $\text{Var}(w(\hat{p})) \approx [w'(p)]^2 \frac{p(1-p)}{G}$  is the variance introduced by weight estimation (Appendix G). Treating updates as independent, we define the per-prompt learning quality  $q(p, w) = s(p)^2 / \text{Var}(w(\hat{p}))$ , the signal-to-noise ratio of the weighted gradient at solve rate  $p$ . The total update quality over the difficulty distribution  $f(p)$  is:

$$\mathcal{Q}(w) = \underbrace{N_{\text{eff}}}_{\text{effective count}} \times \underbrace{\mathbb{E}_{p \sim f}[q(p, w)]}_{\text{per-sample quality}} = N_{\text{eff}} \times \mathbb{E}_{p \sim f} \left[ \frac{s(p)}{\text{Var}(w(\hat{p})\hat{g})} \right] \quad (10)$$

where  $N_{\text{eff}} = M (\mathbb{E}[w])^2 / \mathbb{E}[w^2] \leq M$  is Kish’s effective sample size. Increasing  $\alpha$  selectively filters out easy prompts, which can raise  $q(p, w)$  at the mode but reduces  $N_{\text{eff}}$ .

Since  $w$  must serve all difficulties simultaneously, we seek  $w^* = \arg \max_w \mathcal{Q}(w)$  over the current distribution  $f(p)$ , which may shift over the course of training. In practice, our gradient signal  $s(p)$  is unknown, so we consider two hypotheses. If gradient updates carry the same signal regardless of difficulty ( $s(p) \equiv s$ ), the only lever is variance reduction: the optimal strategy assigns weight proportional to the inverse noise,  $w^*(p) \propto 1/v_0(p) \propto p(1-p)$ , concentrating on medium-difficulty prompts where both successes and failures are frequent enough to yield low-variance gradient estimates. This corresponds to  $\alpha = 1$  (mean GRPO) and is the case for larger models (CWM 32B) (Figure 1).

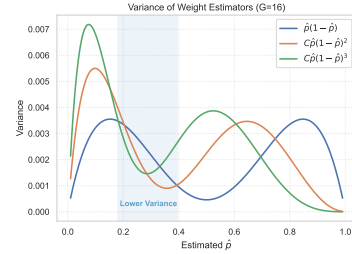


**Figure 7** Variance of the gradient weight  $p(1-p)^\alpha$  at different solve rates for 16 MC rollouts.

If instead harder problems carry a stronger learning signal ( $s'(p) < 0$ ), the optimal filter tilts toward low  $p$  ( $\alpha > 1$ ), placing the weight mode at  $\frac{1}{1+\alpha}$  (see Figure 7). At a solve rate of 0.5,  $\alpha = 3$  is justified only if hard problems carry at least  $2.25\times$  more signal than the average prompt (Table 8). This matches the 7B regime, where Power  $\alpha=2$  gives  $+5\%$  pass@ $k$  over GRPO (Tables 3, 4), suggesting smaller models have more to learn from hard problems. However as the policy improves, problems that once provided signal become easy, and the pool of hard problems shrinks, reducing  $N_{\text{eff}}$  and degrading update quality for large  $\alpha$ . Methods like pass@ $k$  advantages that target tail-end difficulties are especially vulnerable, waiting for signal on unsolvable problems while ignoring steady progress on medium-difficulty prompts (Figure 5).

## 5 The FADE Scheduler

The previous sections revealed two trade-offs that a fixed policy weight cannot satisfy simultaneously:

- **Sign axis** (§4.1, §4.2): failure-biased methods ( $\delta < 1$ ) learn faster but induce rank-1 update collapse; sign-balanced methods ( $\delta = 1$ ) preserve multi-dimensional learning but converge slowly.
- **Difficulty axis** (§4.3): focusing on hard problems maximizes gradient informativeness but at the cost of higher variance and less relevant batches.

To maximize gradient efficiency, we propose to adapt the policy weight to online learning dynamics. Combining Asym GRPO and Power  $\alpha$ , we propose **Focal Advantage with Dynamic Entropy** (FADE) which adapts the policy weight to the moving average of solve rate  $\hat{p}$  and entropy  $\hat{H}$ :

$$A_i = (1 - \bar{r})^{\alpha-1} \cdot \begin{cases} r_i - \bar{r} & \text{if } r_i \geq \bar{r}, \\ \frac{r_i - \bar{r}}{\delta} & \text{if } r_i < \bar{r}, \end{cases} \quad \alpha = \text{clip}\left(\frac{3(1 - \hat{p})}{2\hat{p}}, 1, \alpha_{\text{max}}\right), \quad \delta = \text{clip}(1 + \hat{H} - H^*, 0.3, 1). \quad (11)$$

Algorithm 2 shows how FADE can be used in practice. We found  $\alpha_{\text{max}} = 3$  and a target entropy  $H^*$  of half the initial entropy worked best (Appendix C). FADE can be seen as delayed exploitation. In a typical training run (Figure 8),  $\alpha$  starts high making the policy focus on frontier problems and develop diverse reasoning strategies. When the entropy drops below  $H^*$  we force exploitation by making the gradients failure-biased with  $\delta < 1$ . The initial sign-balanced phase ( $\delta = 1$ ) prevents premature rank-1 collapse in the update weights. On the other hand, the decaying  $\alpha$  power avoids the gradient allocation trap where we overfit to hard problems. Figure 1 shows that FADE achieves the best performance across all pass@ $k$  metrics while reaching peak pass@1 20k steps earlier than the best static baseline (Power  $\alpha=2$ ) at the 7B scale and 2k steps earlier at the 32B scale.

We ablate each component independently (Figure 9): removing  $\delta$  causes entropy collapse while removing  $\alpha$  loses diversity. We also test two simplifications: (1) replacing both signals with a deterministic logarithmic schedule  $f(t) \propto \log(1 + t/\tau)$ , and (2) driving both  $\alpha$  and  $\delta$  from entropy alone. Both degrade diversity (pass@10, pass@100), confirming that  $\alpha$  and  $\delta$  must respond to distinct signals to balance exploration and exploitation effectively.

FADE’s entropy target provides a single interpretable knob controlling the exploration-exploitation in the learned update weights  $W_\Delta$  (see Figure 6). We track the SVD of the output-head weight change  $W_\Delta$  (singular-value ratio  $s_1/s_2$  and rank-1 fraction) alongside its  $L_2$  norm across three FADE runs with  $H^* \in \{0.5, 1.0, 1.3\}$  on Qwen 2.5 7B (Table 8). The result is a clean, continuous transition:  $H^*=0.5$  keeps  $\|W_\Delta\|$  small and the update full-rank;  $H^*=1.0$  grows  $\|W_\Delta\|$  to 67% with moderate rank concentration;  $H^*=1.3$  reproduces the rank-1 collapse seen in static failure-biased methods ( $s_1/s_2 > 5$ , rank-1 fraction 91%).

## 6 Related Works

**Test-time scaling and diversity collapse.** Test-time compute scaling, sampling  $k$  candidate solutions and selecting the best, has become a standard strategy for improving LLM reasoning, through self-consistency (Wang et al., 2023), multi-turn verification (Lightman et al., 2024), or simply majority voting. Brown et al. (2024) and Schaeffer et al. (2025) characterized the resulting pass@ $k$  curves as a power law governed by the distribution of per-problem solve rates. Training-time scaling laws for RL have been studied along complementary

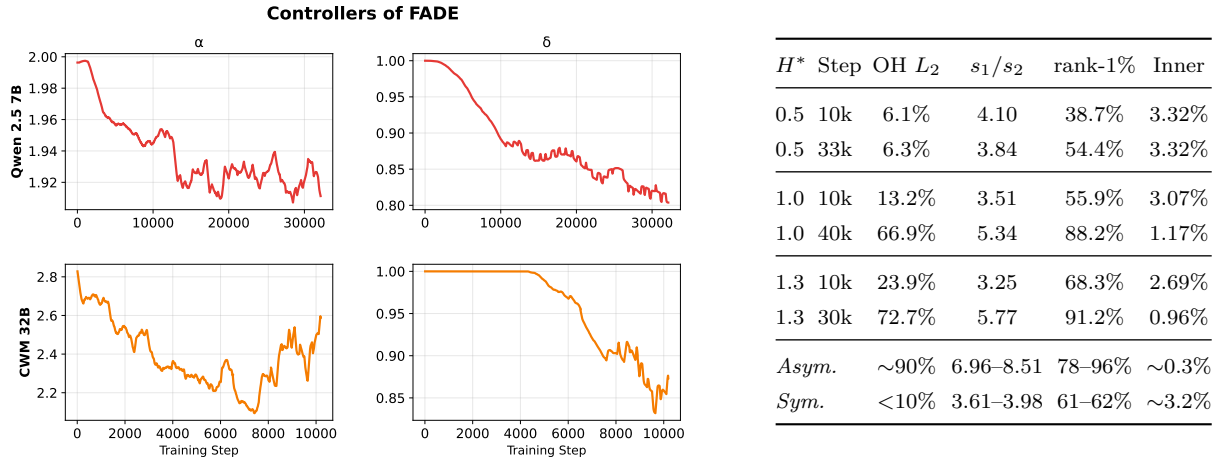


**Figure 8 (Left)** FADE controller dynamics:  $\alpha$  and  $\delta$  adapt the policy gradient weight  $p(1-p)^\alpha/\delta$ ;  $\delta$  decays once entropy hits  $H^*$  and  $\alpha$  decays as solve rates rise. **(Right)** Output-head SVD metrics at different entropy targets confirm that  $H^*$  continuously controls the sign-balanced-to-failure-biased transition (Table 8).

axes: environment interactions (Hilton et al., 2023), entropy budgets (Cui et al., 2025), and algorithmic choices (Khatri et al., 2025; Kaplan et al., 2020; Tan et al., 2025). At the intersection of training and inference, several works observed that RL fine-tuning “sharpens” the policy: pass@1 improves while pass@ $k$  degrades as the model collapses onto a narrow set of solutions (Huang et al., 2025; Karan and Du, 2025; Levi, 2026). Barakat et al. (2026) formalized this as a gradient-level trade-off, showing that pass@1 and pass@ $k$  optimization apply opposing forces on the policy. Focusing on GRPO, Cheng et al. (2026) showed failed trajectories serve as credit assignment for positive tokens.

**Policy weights and advantage functions.** The advantage function (Baird, 1993) separates the effect of an action from the quality of a state and can be estimated via batch-average baselines (Marbach and Tsitsiklis, 2001; Kool et al., 2019; Mnih and Rezaei, 2016), learned value networks (Wang et al., 2016), or GAE (Schulman et al., 2015). Using Monte Carlo rollouts to estimate the value function was popularized by GRPO (Shao et al., 2024; Guo et al., 2025). To preserve test-time diversity, (Amini et al., 2024; Chow et al., 2024; Walder and Karkhanis, 2025; Tang et al., 2025) propose pass@ $k$  reweighting. Other works design policy weights based on likelihood (Tajwar et al., 2026), sign reweighting (Zhu et al., 2025; He et al., 2025), or more complex proxies such as the top- $k$  redistribution (Peng et al., 2025), or in-context guidance (Qu et al., 2026). Beyond fixed policy weights, The Microsoft AI Team (2026) adjust the upper clip bound to maintain a target policy entropy similar our  $\delta$  scheduler in FADE but at the PPO clipping level. Zhao et al. (2026) directly rescale the GRPO weight based on the average entropy. Our framework is inspired by Thrampoulidis et al. (2025), Chen et al. (2025) and Davis and Recht (2025), who analyze the reward shaping of advantage functions and their gradient weights. We extend this line of work to a broader range of advantages identifying general structural properties validated via large scale RL experiments.

**Weight-space analysis of RL training.** Kumar et al. (2020) studied rank collapse in Q-learning with gradient descent, attributing it to bootstrapping. In contrast, we’re interested in the rank of the update weight since in RL with LLMs we have relatively few changes in the model weights. Cai et al. (2025) observed rank-1 dominance of the parameter update matrix, more pronounced in RL than in SFT or distillation. Ye et al. (2026) showed that non-rank-1 directions encode out-of-domain abilities beyond reasoning, framing rank-1 collapse as a form of overfitting. Moalla et al. (2024) showed update weights become lower rank in high-entropy regimes correlating with our observations for  $\delta > 1$ .

## 7 Conclusion

By decomposing policy weights into their positive and negative gradient masses ( $m_S$ ,  $m_F$ ), we revealed two orthogonal axes that jointly govern training dynamics. Balancing the sign balance of  $m_S$  and  $m_F$  can push

the policy to entropy collapse if  $m_S \gg m_F$  or rank-1 update collapse if  $m_F \gg m_S$ , accelerating training at the cost of less diverse features. On the other hand, looking at  $m_S(p), m_F(p)$  so the policy gradient mass as functions of the batch’s solve rate  $p$ , we showed another trade-off between the signal to noise per batch. Combining these two directions, we notice two paradigms: the explorative mode where we should have a balanced sign ratio and focus on hard problems; and the exploitative mode where we want fast learning and no variance.

Building on this analysis, we introduced FADE, which adapts both axes to online training dynamics. It reaches peak pass@1 20k steps earlier than the best static baseline at 7B and 2k steps earlier at 32B, while maintaining the best diversity-accuracy trade-off across models and benchmarks (LiveCodeBench, AIME).

Several directions remain open. Our framework assumes binary, terminal rewards; extending the  $m_S/m_F$  decomposition to process reward models with per-step credit assignment would clarify whether the sign and difficulty trade-offs persist at finer granularity. Similarly, when only a few Monte Carlo rollouts per prompt are available, the estimate  $\bar{p}$  becomes noisy. Understanding which policy weights are robust to this estimation error, and how the optimal choice shifts in the low-rollout regime, deserves further study. Finally, all experiments use single-turn code and math generation; multi-turn and agentic settings, where intermediate feedback is available, may shift the exploration-exploitation balance in ways our trajectory-level analysis does not capture.

## References

- Wasi Uddin Ahmad, Somshubra Majumdar, Aleksander Ficek, Sean Narenthiran, Mehrzad Samadi, Jocelyn Huang, Siddhartha Jain, Vahid Noroozi, and Boris Ginsburg. Opencodereasoning-ii: A simple test time scaling approach via self-critique. *arXiv preprint arXiv:2507.09075*, 2025.
- Arash Ahmadian, Chris Cremer, Matthias Gallé, Marzieh Fadaee, Julia Kreutzer, Olivier Pietquin, Ahmet Üstün, and Sara Hooker. Back to basics: Revisiting reinforce-style optimization for learning from human feedback in llms. In *Proceedings of the 62nd Annual Meeting of the Association for Computational Linguistics (Volume 1: Long Papers)*, pages 12248–12267, 2024.
- Afra Amini, Tim Vieira, Elliott Ash, and Ryan Cotterell. Variational best-of-n alignment. *arXiv preprint arXiv:2407.06057*, 2024.
- Marcin Andrychowicz, Anton Raichuk, Piotr Stańczyk, Manu Orsini, Sertan Girgin, Raphaël Marinier, Léonard Hussenot, Matthieu Geist, Olivier Pietquin, Marcin Michalski, et al. What matters in on-policy reinforcement learning? a large-scale empirical study. In *ICLR 2021-Ninth International Conference on Learning Representations*, 2021.
- Charles Arnal, Gaëtan Narozniak, Vivien Cabannes, Yunhao Tang, Julia Kempe, and Remi Munos. Asymmetric reinforce for off-policy reinforcement learning: Balancing positive and negative rewards. *Advances in Neural Information Processing Systems*, 38:9640–9664, 2026.
- Leemon C Baird. Advantage updating. Technical report, Wright Laboratory, 1993.
- Anas Barakat, Souradip Chakraborty, Khushbu Pahwa, and Amrit Singh Bedi. Why pass@ k optimization can degrade pass@ 1: Prompt interference in llm post-training. *arXiv preprint arXiv:2602.21189*, 2026.
- Bradley Brown, Jordan Juravsky, Ryan Ehrlich, Ronald Clark, Quoc V Le, Christopher Ré, and Azalia Mirhoseini. Large language monkeys: Scaling inference compute with repeated sampling. *arXiv preprint arXiv:2407.21787*, 2024.
- Yuchen Cai, Ding Cao, Xin Xu, Zijun Yao, Yuqing Huang, Zhenyu Tan, Benyi Zhang, Guangzhong Sun, Guiquan Liu, and Junfeng Fang. On predictability of reinforcement learning dynamics for large language models. *arXiv preprint arXiv:2510.00553*, 2025.
- Mark Chen, Jerry Tworek, Heewoo Jun, Qiming Yuan, Henrique Ponde De Oliveira Pinto, Jared Kaplan, Harri Edwards, Yuri Burda, Nicholas Joseph, Greg Brockman, et al. Evaluating large language models trained on code. *arXiv preprint arXiv:2107.03374*, 2021.
- Zhipeng Chen, Xiaobo Qin, Youbin Wu, Yue Ling, Qinghao Ye, Wayne Xin Zhao, and Guang Shi. Pass@ k training for adaptively balancing exploration and exploitation of large reasoning models. *arXiv preprint arXiv:2508.10751*, 2025.
- Tianhao Cheng, Zeyu Huang, Zihan Qiu, Yu Cheng, Edoardo Ponti, Yinghui Xu, Ivan Titov, and Zenglin Xu. The cancellation hypothesis in critic-free rl: From outcome rewards to token credits. *arXiv preprint arXiv:2605.08666*, 2026.
- Yinlam Chow, Guy Tennenholtz, Izzeddin Gur, Vincent Zhuang, Bo Dai, Sridhar Thiagarajan, Craig Boutilier, Rishabh Agarwal, Aviral Kumar, and Aleksandra Faust. Inference-aware fine-tuning for best-of-n sampling in large language models. *arXiv preprint arXiv:2412.15287*, 2024.
- Ganqu Cui, Yuchen Zhang, Jiacheng Chen, Lifan Yuan, Zhi Wang, Yuxin Zuo, Haozhan Li, Yuchen Fan, Huayu Chen, Weize Chen, et al. The entropy mechanism of reinforcement learning for reasoning language models. *arXiv preprint arXiv:2505.22617*, 2025.
- Will Dabney, Mark Rowland, Marc Bellemare, and Rémi Munos. Distributional reinforcement learning with quantile regression. In *Proceedings of the AAAI conference on artificial intelligence*, volume 32, 2018.
- Damek Davis and Benjamin Recht. What is the objective of reasoning with reinforcement learning? *arXiv preprint arXiv:2510.13651*, 2025.
- FAIR CodeGen team, :, Jade Copet, Quentin Carbonneaux, Gal Cohen, Jonas Gehring, Jacob Kahn, Jannik Kossen, Felix Kreuk, Emily McMilin, Michel Meyer, Yuxiang Wei, David Zhang, Kunhao Zheng, Jordi Armengol-Estapé, Pedram Bashiri, Maximilian Beck, Pierre Chambon, Abhishek Charnalia, Chris Cummins, Juliette Decugis, Zacharias V. Fisches, François Fleuret, Fabian Gloeckle, Alex Gu, Michael Hassid, Daniel Haziza, Badr Youbi Idrissi, Christian Keller, Rahul Kindi, Hugh Leather, Gallil Maimon, Aram Markosyan, Francisco Massa, Pierre-Emmanuel

- Mazaré, Vegard Mella, Naila Murray, Keyur Muzumdar, Peter O’Hearn, Matteo Pagliardini, Dmitrii Pedchenko, Tal Remez, Volker Seeker, Marco Selvi, Oren Sultan, Sida Wang, Luca Wehrstedt, Ori Yoran, Lingming Zhang, Taco Cohen, Yossi Adi, and Gabriel Synnaeve. Cwm: An open-weights llm for research on code generation with world models. *arXiv preprint arXiv:2510.02387*, 2025.
- Yulu Gan and Phillip Isola. Neural thicketts: Diverse task experts are dense around pretrained weights. *arXiv preprint arXiv:2603.12228*, 2026.
- Anisha Garg and Ganesh Venkatesh. The peril of preference: Why grpo fails on ordinal rewards. *arXiv preprint arXiv:2511.04439*, 2025.
- Jonas Gehring, Kunhao Zheng, Jade Copet, Vegard Mella, Taco Cohen, and Gabriel Synnaeve. Rlef: Grounding code llms in execution feedback with reinforcement learning. In *International Conference on Machine Learning*, pages 19034–19055. PMLR, 2025.
- Evan Greensmith, Peter L Bartlett, and Jonathan Baxter. Variance reduction techniques for gradient estimates in reinforcement learning. *Journal of Machine Learning Research*, 5(Nov):1471–1530, 2004.
- Daya Guo, Dejian Yang, Haowei Zhang, Junxiao Song, Peiyi Wang, Qihao Zhu, Runxin Xu, Ruoyu Zhang, Shirong Ma, Xiao Bi, et al. Deepseek-r1 incentivizes reasoning in llms through reinforcement learning. *Nature*, 645(8081): 633–638, 2025.
- Andre Wang He, Daniel Fried, and Sean Welleck. Rewarding the unlikely: Lifting grpo beyond distribution sharpening. In *Proceedings of the 2025 Conference on Empirical Methods in Natural Language Processing*, pages 25559–25571, 2025.
- Jacob Hilton, Jie Tang, and John Schulman. Scaling laws for single-agent reinforcement learning. *arXiv preprint arXiv:2301.13442*, 2023.
- Audrey Huang, Adam Block, Dylan Foster, Dhruv Rohatgi, Cyril Zhang, Max Simchowitz, Jordan Ash, and Akshay Krishnamurthy. Self-improvement in language models: The sharpening mechanism. In *International Conference on Learning Representations*, volume 2025, pages 76687–76739, 2025.
- Binyuan Hui, Jian Yang, Zeyu Cui, Jiayi Yang, Dayiheng Liu, Lei Zhang, Tianyu Liu, Jiajun Zhang, Bowen Yu, Keming Lu, et al. Qwen2. 5-coder technical report. *arXiv preprint arXiv:2409.12186*, 2024.
- Yuhua Jiang, Jiawei Huang, Yufeng Yuan, Xin Mao, Yu Yue, Qianchuan Zhao, and Lin Yan. Risk-sensitive rl for alleviating exploration dilemmas in large language models. *arXiv preprint arXiv:2509.24261*, 2025.
- Jared Kaplan, Sam McCandlish, Tom Henighan, Tom B. Brown, Benjamin Chess, Rewon Child, Scott Gray, Alec Radford, Jeffrey Wu, and Dario Amodei. Scaling laws for neural language models. *arXiv preprint arXiv:2001.08361*, 2020.
- Aayush Karan and Yilun Du. Reasoning with sampling: Your base model is smarter than you think. *arXiv preprint arXiv:2510.14901*, 2025.
- Devvrit Khatrri, Lovish Madaan, Rishabh Tiwari, Rachit Bansal, Sai Surya Duvvuri, Manzil Zaheer, Inderjit S Dhillon, David Brandfonbrener, and Rishabh Agarwal. The art of scaling reinforcement learning compute for llms. *arXiv preprint arXiv:2510.13786*, 2025.
- Youngeun Kim. Mc-grpo: Median-centered group relative policy optimization for small-rollout reinforcement learning. *arXiv preprint arXiv:2601.22582*, 2026.
- Kimi Team, Angang Du, Bofei Gao, Bofei Xing, Changjiu Jiang, Cheng Chen, Cheng Li, Chenjun Xiao, Chenzhuang Du, Chonghua Liao, et al. Kimi k1. 5: Scaling reinforcement learning with llms. *arXiv preprint arXiv:2501.12599*, 2025.
- Wouter Kool, Herke van Hoof, and Max Welling. Buy 4 reinforce samples, get a baseline for free! *arXiv preprint arXiv:1901.10280*, 2019.
- Aviral Kumar, Rishabh Agarwal, Dibya Ghosh, and Sergey Levine. Implicit under-parameterization inhibits data-efficient deep reinforcement learning. *arXiv preprint arXiv:2010.14498*, 2020.
- Noam Levi. Learning shrinks the hard tail: Training-dependent inference scaling in a solvable linear model. *arXiv preprint*, 2026.
- Rongao Li, Jie Fu, Bo-Wen Zhang, Tao Huang, Zhihong Sun, Chen Lyu, Guang Liu, Zhi Jin, and Ge Li. Taco: Topics in algorithmic code generation dataset. *arXiv preprint arXiv:2312.14852*, 2023.

- Yujia Li, David Choi, Junyoung Chung, Nate Kushman, Julian Schrittwieser, Rémi Leblond, Tom Eccles, James Keeling, Felix Gimeno, Agustin Dal Lago, et al. Competition-level code generation with alphacode. *Science*, 378(6624):1092–1097, 2022.
- Hunter Lightman, Vineet Kosaraju, Yuri Burda, Harrison Edwards, Bowen Baker, Teddy Lee, Jan Leike, John Schulman, Ilya Sutskever, and Karl Cobbe. Let’s verify step by step. In *The Twelfth International Conference on Learning Representations*, 2024.
- Tsung-Yi Lin, Priya Goyal, Ross Girshick, Kaiming He, and Piotr Dollár. Focal loss for dense object detection. In *Proceedings of the IEEE international conference on computer vision*, pages 2980–2988, 2017.
- Wenze Lin, Zhen Yang, Xitai Jiang, Pony Ma, and Gao Huang. Thickening-to-thinning: Reward shaping via human-inspired learning dynamics for llm reasoning. *arXiv preprint arXiv:2602.04265*, 2026.
- Zi-Yan Liu, Changyu Chen, Wenjun Li, Penghui Qi, Tianyu Pang, Chao Du, Wee Sun Lee, and Min Lin. Understanding r1-zero-like training: A critical perspective. *ArXiv*, abs/2503.20783, 2025a.
- Zichen Liu, Changyu Chen, Wenjun Li, Penghui Qi, Tianyu Pang, Chao Du, Wee Sun Lee, and Min Lin. Understanding r1-zero-like training: A critical perspective. *arXiv preprint arXiv:2503.20783*, 2025b.
- Peter Marbach and John N Tsitsiklis. Simulation-based optimization of markov reward processes. *IEEE Transactions on Automatic Control*, 46(2):191–209, 2001.
- Marvin Minsky. Steps toward artificial intelligence. *Proceedings of the IRE*, 49(1):8–30, 1961.
- Andriy Mnih and Danilo Rezende. Variational inference for monte carlo objectives. In *International Conference on Machine Learning*, pages 2188–2196. PMLR, 2016.
- Skander Moalla, Andrea Miele, Daniil Pyatko, Razvan Pascanu, and Caglar Gulcehre. No representation, no trust: Connecting representation, collapse, and trust issues in ppo. *Advances in Neural Information Processing Systems*, 37:69652–69699, 2024.
- Ivan Moshkov, Darragh Hanley, Ivan Sorokin, Shubham Toshniwal, Christof Henkel, Benedikt Schifferer, Wei Du, and Igor Gitman. Aimo-2 winning solution: Building state-of-the-art mathematical reasoning models with open-mathreasoning dataset. *arXiv preprint arXiv:2504.16891*, 2025.
- Michael Noukhovitch, Shengyi Huang, Sophie Xhonneux, Arian Hosseini, Rishabh Agarwal, and Aaron Courville. Asynchronous rlhf: Faster and more efficient off-policy rl for language models. In *International Conference on Learning Representations*, volume 2025, pages 4003–4029, 2025.
- OpenAI. Learning to reason with LLMs. <https://openai.com/index/learning-to-reason-with-llms/>, September 2024.
- Jaesung R Park, Junsu Kim, Gyeongman Kim, Jinyoung Jo, Sean Choi, Jaewoong Cho, and Ernest K Ryu. Clip-low increases entropy and clip-high decreases entropy in reinforcement learning of large language models. *arXiv preprint arXiv:2509.26114*, 2025.
- Ruotian Peng, Yi Ren, Zhouliang Yu, Weiyang Liu, and Yandong Wen. Simko: Simple pass@ k policy optimization. *arXiv preprint arXiv:2510.14807*, 2025.
- Daniil Plyusov, Alexey Gorbatoevski, Boris Shaposhnikov, Viacheslav Sinii, Alexey Malakhov, and Daniil Gavrilov. F-grpo: Don’t let your policy learn the obvious and forget the rare. *arXiv preprint arXiv:2602.06717*, 2026.
- Yuxiao Qu, Amrith Setlur, Virginia Smith, Ruslan Salakhutdinov, and Aviral Kumar. Pope: Learning to reason on hard problems via privileged on-policy exploration. *arXiv preprint arXiv:2601.18779*, 2026.
- Rylan Schaeffer, Joshua Kazdan, John Hughes, Jordan Juravsky, Sara Price, Aengus Lynch, Erik Jones, Robert Kirk, Azalia Mirhoseini, and Sanmi Koyejo. How do large language monkeys get their power (laws)? In *International Conference on Machine Learning*, pages 53132–53176. PMLR, 2025.
- John Schulman, Philipp Moritz, Sergey Levine, Michael Jordan, and Pieter Abbeel. High-dimensional continuous control using generalized advantage estimation. *arXiv preprint arXiv:1506.02438*, 2015.
- John Schulman, Filip Wolski, Prafulla Dhariwal, Alec Radford, and Oleg Klimov. Proximal policy optimization algorithms. *arXiv preprint arXiv:1707.06347*, 2017.
- Zhihong Shao, Peiyi Wang, Qihao Zhu, Runxin Xu, Junxiao Song, Xiao Bi, Haowei Zhang, Mingchuan Zhang, YK Li, et al. Deepseekmath: Pushing the limits of mathematical reasoning in open language models. *arXiv preprint arXiv:2402.03300*, 2024.

- Sriram Srinivasan, Marc Lanctot, Vinicius Zambaldi, Julien Pérolat, Karl Tuyls, Rémi Munos, and Michael Bowling. Actor-critic policy optimization in partially observable multiagent environments. *Advances in Neural Information Processing Systems*, 31, 2018.
- Joe Suk and Yaqi Duan. On the optimization dynamics of rlvr: Gradient gap and step size thresholds. *arXiv preprint arXiv:2510.08539*, 2025.
- Richard S Sutton. Learning to predict by the methods of temporal differences. *Machine learning*, 3(1):9–44, 1988.
- Richard S. Sutton, David McAllester, Satinder Singh, and Yishay Mansour. Policy gradient methods for reinforcement learning with function approximation. In *Proceedings of the 13th International Conference on Neural Information Processing Systems (NIPS)*, pages 1057–1063, Cambridge, MA, USA, 1999. MIT Press.
- Fahim Tajwar, Guanning Zeng, Yuer Zhou, Yuda Song, Daman Arora, Yiding Jiang, Jeff Schneider, Ruslan Salakhutdinov, Haiwen Feng, and Andrea Zanette. Maximum likelihood reinforcement learning. *arXiv preprint arXiv:2602.02710*, 2026.
- Zelin Tan, Hejia Geng, Xiaohang Yu, Mulei Zhang, Guancheng Wan, Yifan Zhou, Qiang He, Xiangyuan Xue, Heng Zhou, Yutao Fan, et al. Scaling behaviors of llm reinforcement learning post-training: An empirical study in mathematical reasoning. *arXiv preprint arXiv:2509.25300*, 2025.
- Yunhao Tang, Kunhao Zheng, Gabriel Synnaeve, and Rémi Munos. Optimizing language models for inference time objectives using reinforcement learning. *arXiv preprint arXiv:2503.19595*, 2025.
- The Microsoft AI Team. Mai-thinking-1: Building a hill-climbing machine. Technical report, Microsoft AI, 2026. <https://microsoft.ai/pdf/mai-thinking-1.pdf>.
- Christos Thrampoulidis, Sadegh Mahdavi, and Wenlong Deng. Advantage shaping as surrogate reward maximization: Unifying pass@k policy gradients. *arXiv preprint arXiv:2510.23049*, 2025.
- Christian Walder and Deep Karkhanis. Pass@k policy optimization: Solving harder reinforcement learning problems. *arXiv preprint arXiv:2505.15201*, 2025.
- Xuezhi Wang, Jason Wei, Dale Schuurmans, Quoc V Le, Ed H Chi, Sharan Narang, Aakanksha Chowdhery, and Denny Zhou. Self-consistency improves chain of thought reasoning in language models. In *The Eleventh International Conference on Learning Representations*, 2023.
- Ziyu Wang, Tom Schaul, Matteo Hessel, Hado Hasselt, Marc Lanctot, and Nando Freitas. Dueling network architectures for deep reinforcement learning. In *International conference on machine learning*, pages 1995–2003. PMLR, 2016.
- Ronald J. Williams. Simple statistical gradient-following algorithms for connectionist reinforcement learning. *Machine Learning*, 8(3–4):229–256, 1992. doi: 10.1007/BF00992696.
- Xue Yan, Yan Song, Xidong Feng, Mengyue Yang, Haifeng Zhang, Haitham Bou Ammar, and Jun Wang. Efficient reinforcement learning with large language model priors. In *International Conference on Learning Representations*, volume 2025, pages 48691–48715, 2025.
- Fengkai Yang, Zherui Chen, Xiaohan Wang, Xiaodong Lu, Jiajun Chai, Guojun Yin, Wei Lin, Shuai Ma, Fuzhen Zhuang, Deqing Wang, et al. Your group-relative advantage is biased. *arXiv preprint arXiv:2601.08521*, 2026.
- Hao Ye, Jisheng Dang, Junfeng Fang, Bimei Wang, Yizhou Zhang, Ning Lv, Wencan Zhang, Hong Peng, Bin Hu, and Tat-Seng Chua. On the implicit reward overfitting and the low-rank dynamics in rlvr. *arXiv preprint arXiv:2605.06523*, 2026.
- Qiyang Yu, Zheng Zhang, Ruofei Zhu, Yufeng Yuan, Xiaochen Zuo, Yu Yue, Weinan Dai, Tiantian Fan, Gaohong Liu, Lingjun Liu, et al. Dapo: An open-source llm reinforcement learning system at scale. *arXiv preprint arXiv:2503.14476*, 2025.
- Chenchen Zhang. From reasoning to agentic: Credit assignment in reinforcement learning for large language models. *arXiv preprint arXiv:2604.09459*, 2026.
- Haotian Zhao, Songlin Zhou, Yuxin Zhang, Stephen S-T Yau, Wenyu Zhang, Lun Tian, Tianshu Zhu, Yifeng Huang, Yucheng Zeng, Jingnan Gu, et al. Aem: Adaptive entropy modulation for multi-turn agentic reinforcement learning. *arXiv preprint arXiv:2605.00425*, 2026.
- Xinyu Zhu, Mengzhou Xia, Zhepei Wei, Wei-Lin Chen, Danqi Chen, and Yu Meng. The surprising effectiveness of negative reinforcement in llm reasoning. *arXiv preprint arXiv:2506.01347*, 2025.

# Appendix

## A Deriving Positive and Negative Weights

Throughout,  $\tau_S$  and  $\tau_F$  denote successful and failed trajectories (positive and negative weights),  $\bar{r} := \frac{1}{B} \sum_i r_i$  the batch reward mean,  $\sigma_r = \sqrt{\frac{1}{B} \sum_i (r_i - \bar{r})^2}$  the reward standard deviation, and all gradients are estimated over  $B$  independent rollouts from  $\pi_\theta$ .

### A.1 GRPO

The GRPO advantage is  $A_i = (r_i - \bar{r})/\sigma_r$ . For binary rewards  $r_i \in \{0, 1\}$  with  $\bar{r} = \hat{p}$ , the empirical standard deviation reduces to the Bernoulli form  $\sigma_r = \sqrt{\hat{p}(1 - \hat{p})} = \sqrt{pq}$ , since:

$$\sigma_r^2 = \frac{1}{B} \sum_{i=1}^B (r_i - \hat{p})^2 = \frac{1}{B} [Bp(1-p)^2 + Bqp^2] = pq(q+p) = pq.$$

The per-trajectory advantages are:

$$A_s = \frac{q}{\sqrt{pq}} = \sqrt{\frac{q}{p}}, \quad A_f = \frac{-p}{\sqrt{pq}} = -\sqrt{\frac{p}{q}}.$$

With  $|S| = Bp$  and  $|F| = Bq$  in expectation:

$$\nabla_{\text{GRPO}} = \frac{q}{\sqrt{pq}} \cdot Bp \cdot \mathbf{m}_S - \frac{p}{\sqrt{pq}} \cdot Bq \cdot \mathbf{m}_F = \frac{Bpq}{\sqrt{pq}} [\mathbf{m}_S - \mathbf{m}_F] = B\sqrt{pq} [\mathbf{m}_S - \mathbf{m}_F].$$

Hence  $m_S = m_F = Bpq/\sigma_r = B\sqrt{pq}$ , confirming sign balance. Skew-R introduced by [Thrampoulidis et al. \(2025\)](#) combines regular and mean based GRPO by taking the product of both giving  $m_S = m_F = pq \times \sqrt{pq}$ .

### A.2 Multiplier Rescaled GRPO

The  $\frac{1}{\sigma_r}$  multiplier in GRPO is unstable ([Liu et al., 2025b](#)) ([Yu et al., 2025](#)), as it can lead to exploding or noisy gradient updates. Instead, we can keep the mean normalization and introduce other multipliers:

$$\nabla_{\text{rescale}} = \sum_{i \in S} C_s(\mathbf{r}, i) \cdot (r_i - \bar{r}) \nabla \log \pi_\theta(\tau_i) - \sum_{i \in F} C_f(\mathbf{r}, i) \cdot (\bar{r} - r_i) \nabla \log \pi_\theta(\tau_i),$$

where  $C_s(\mathbf{r}, i)$  and  $C_f(\mathbf{r}, i)$  are arbitrary non-negative functions that may depend on the full reward vector  $\mathbf{r} = (r_1, \dots, r_B)$  and the sample index  $i$ . Mirroring the logic behind the focal loss ([Lin et al., 2017](#)), we introduce the power  $\alpha$  series (PA) where the functions are powers of  $|r_i - \bar{r}|$ .

Our proposed methods:

1. **Power  $\alpha$  (sign-balanced):** The intuition is to reduce the gradient magnitude when the model already performs well ( $\bar{r}$  high): samples that are easy to solve should contribute less to the update. We set  $C_s(\mathbf{r}, i) = C_f(\mathbf{r}, i) = (1 - \bar{r})^{\alpha-1}$  for all  $i$ , so the advantage becomes:

$$\hat{A}_i = (r_i - \bar{r})(1 - \bar{r})^{\alpha-1}.$$

For binary rewards where  $\bar{r} = p$ , this simplifies to  $C_s = C_f = q^{\alpha-1}$ , giving:

$$m_S = m_F = Bpq \cdot q^{\alpha-1} = Bpq^\alpha.$$

As  $\alpha$  increases, the masses decay faster with  $q$ : gradients are suppressed on prompts the model has mostly solved, focusing optimization on harder problems.

2. **Asymmetric Power  $\alpha$ :** We decouple the exponents:  $C_s(\mathbf{r}, i) = (1 - \bar{r})^{\alpha_s-1}$  for  $i \in S$  and  $C_f(\mathbf{r}, i) = \bar{r}^{\alpha_f-1}$  for  $i \in F$ . The positive mass derivation is identical to the sign-balanced case:

$$m_S = Bpq^{\alpha_s}.$$

For the negative side, with binary rewards  $\bar{r} = p$ :

$$m_F = Bp^{\alpha_f - 1} \cdot p \cdot q = Bp^{\alpha_f} q.$$

If  $\alpha_s > \alpha_f$  we suppress the positive gradient more than the negative one (or vice versa), giving explicit control over the diversity–performance tradeoff. Note that  $\alpha_s = \alpha_f = 1$  recovers GRPO ( $m_S = m_F = pq$ ).

3. **Asymmetric GRPO:** keeps the GRPO advantage intact on the positive side and rescales only the negative side by a fixed scalar  $\frac{1}{\delta}$ :  $C_s = 1$  and  $C_f = \frac{1}{\delta}$ . This gives:

$$m_S = Bpq, \quad m_F = \frac{Bpq}{\delta}.$$

When  $\delta < 1$ , the negative gradient is amplified relative to the positive one ( $m_F > m_S$ ), pushing the model more aggressively away from failed trajectories. When  $\delta > 1$ , the negative gradient is suppressed ( $m_F < m_S$ ), preserving diversity by reducing the penalty on incorrect solutions. At  $\delta = 1$  we recover standard GRPO. Unlike Power  $\alpha$ , this method does not adapt to the difficulty of the prompt ( $p$ ). It modifies only the strength of negative advantages.

**Thickening to Thinning (T2T)** propose another type of  $C_s$  and  $C_f$  multiplier for GRPO based on the average normalized lengths of successful and failed responses,  $\bar{L}_S$  and  $\bar{L}_F$ . They define the reward as  $R_i = \begin{cases} 1 - \alpha p L_i & \text{if } \mathcal{V}_i = 1 \\ \alpha(1 - p)L_i & \text{if } \mathcal{V}_i = 0 \end{cases}$  within a GRPO normalization. The batch mean is:

$$\mu = \frac{1}{B} (\sum_{i \in S} (1 - \alpha p L_i) + \sum_{j \in F} \alpha(1 - p)L_j) = p - \alpha p^2 \bar{L}_S + \alpha(1 - p)^2 \bar{L}_F. \quad (12)$$

Defining  $C := 1 - \alpha p \bar{L}_S - \alpha(1 - p)\bar{L}_F$ , the positive and negative advantages are:

$$\bar{A}_S = \frac{1}{\sigma_R} ((1 - \alpha p \bar{L}_S) - \mu) = \frac{(1 - p)}{\sigma_R} [1 - \alpha p \bar{L}_S - \alpha(1 - p)\bar{L}_F] = \frac{(1 - p)C}{\sigma_R}, \quad (13)$$

$$\bar{A}_F = \frac{1}{\sigma_R} (\alpha(1 - p)\bar{L}_F - \mu) = \frac{-p}{\sigma_R} [1 - \alpha p \bar{L}_S - \alpha(1 - p)\bar{L}_F] = \frac{-pC}{\sigma_R}. \quad (14)$$

The gradient takes the form:

$$\nabla_{\text{GRPO-T2T}} \approx \frac{Bp(1 - p)C}{\sigma_R} [\bar{\nabla}_S - \bar{\nabla}_F]$$

### A.3 Maximum Likelihood RL

As introduced in [Tajwar et al. \(2026\)](#), the MaxRL advantage is  $A = \frac{r_i - \bar{r}}{\bar{r}}$ . With  $r \in \{0, 1\}$ , we have  $A_s = \frac{1 - p}{p}$  and  $A_f = \frac{0 - p}{p} = -1$ . Similar to the GRPO gradient we can write:

$$\begin{aligned} \nabla_{\text{MaxRL}} &= \sum_{\tau_s \in S} A_s \nabla \log \pi_\theta(\tau_s) + \sum_{\tau_f \in F} A_f \nabla \log \pi_\theta(\tau_f) \\ &= \frac{1 - p}{p} \sum_{\tau_s \in S} \nabla \log \pi_\theta(\tau_s) - \sum_{\tau_f \in F} \nabla \log \pi_\theta(\tau_f) \\ &= \frac{(1 - p)}{p} \cdot Bp \cdot \mathbf{m}_S - B(1 - p) \cdot \mathbf{m}_F = B(1 - p) [\mathbf{m}_S - \mathbf{m}_F]. \end{aligned}$$

### A.4 Pass@ $k$ Based Methods

#### A.4.1 Pass@ $k$ (Tang et al.)

The leave-one-out advantage of [Tang et al. \(2025\)](#) is  $A_i = \max_k(\mathbf{r}) - \max_k(\mathbf{r}_{-i})$ , where  $\max_k(\mathbf{r}) = \mathbf{1}[\exists j : r_j = 1]$  is the pass@ $k$  indicator over a group of  $k$  samples and  $\mathbf{r}_{-i}$  excludes sample  $i$ .

*Failed samples* ( $r_i = 0$ ). Removing a zero does not change the maximum:  $\max_k(\mathbf{r}) = \max_k(\mathbf{r}_{-i})$  regardless of the other samples, so  $A_i = 0$  for all  $i \in F$ .

Successful samples ( $r_i = 1$ ). We have  $\max_k(\mathbf{r}) = 1$ . The leave-one-out is  $\max_k(\mathbf{r}_{-i}) = \mathbf{1}[\exists j \neq i : r_j = 1]$ , so:

$$A_i = 1 - \mathbf{1}[\exists j \neq i : r_j = 1] = \mathbf{1}[\text{sample } i \text{ is the only success}].$$

Hence  $A_i = 1$  when  $|S| = 1$  and  $i$  is the unique success, and  $A_i = 0$  when  $|S| \geq 2$ .

*Gradient.* Since only the unique-success case contributes:

$$\nabla = \sum_{i=1}^k A_i \nabla \log \pi_\theta(\tau_i) = \begin{cases} \nabla \log \pi_\theta(\tau_s) = \mathbf{m}_S & \text{if } |S| = 1, \\ 0 & \text{otherwise.} \end{cases}$$

Taking expectations,  $\Pr[|S| = 1] = \binom{k}{1} p q^{k-1} = k p q^{k-1}$ , so:

$$\mathbb{E}[\nabla] = k p q^{k-1} \mathbf{m}_S - 0 \cdot \mathbf{m}_F,$$

giving  $m_S = k p q^{k-1}$  and  $m_F = 0$ .

Unlike the sign-balanced methods (where the masses are deterministic for any fixed batch), here the gradient is zero in most batches and only fires when exactly one of  $k$  samples succeeds.

#### A.4.2 Analytical Pass@ $k$ (Chen et al.)

Chen et al. (2025) define the group pass@ $k$  estimator  $R_k = 1 - \binom{F}{k} / \binom{G}{k}$  over  $G$  rollouts with  $F$  failures and  $S = G - F$  successes, with  $\sigma_k = \sqrt{R_k(1 - R_k)}$ . The per-sample advantages are:

$$A_s = \frac{1 - R_k}{\sigma_k}, \quad A_f = \frac{1}{\sigma_k} \left( 1 - R_k - \frac{\binom{F-1}{k-1}}{\binom{G-1}{k-1}} \right).$$

*Simplification.* Define  $Q'_{k-1} := \binom{F-1}{k-1} / \binom{G-1}{k-1}$ . The identity  $\binom{F}{k} / \binom{G}{k} = (F/G) Q'_{k-1}$  gives  $1 - R_k = \hat{q} Q'_{k-1}$ , so:

$$A_s = \frac{\hat{q} Q'_{k-1}}{\sigma_k}, \quad A_f = \frac{Q'_{k-1}(\hat{q} - 1)}{\sigma_k} = \frac{-\hat{p} Q'_{k-1}}{\sigma_k}.$$

Both cases unify into  $A_i = Q'_{k-1}(r_i - \hat{p}) / \sigma_k$ , which is exact for any finite  $G$  and has the  $C \cdot (r_i - \hat{p})$  structure guaranteeing sign balance. Following the GRPO pattern with  $|S| = G\hat{p}$  and  $|F| = G\hat{q}$ :

$$\nabla = \frac{\hat{q} Q'_{k-1}}{\sigma_k} \cdot S \cdot \mathbf{m}_S - \frac{\hat{p} Q'_{k-1}}{\sigma_k} \cdot F \cdot \mathbf{m}_F = \frac{G\hat{p}\hat{q} Q'_{k-1}}{\sigma_k} [\mathbf{m}_S - \mathbf{m}_F].$$

Substituting  $Q'_{k-1} = (1 - R_k) / \hat{q}$  and  $\sigma_k = \sqrt{R_k(1 - R_k)}$ :

$$m_S = m_F = \hat{p} \frac{1 - R_k}{\sigma_k} = \hat{p} \sqrt{\frac{1 - R_k}{R_k}}.$$

At  $k = 1$ ,  $R_1 = S/G = \hat{p}$ , so  $m_S = m_F = \sqrt{\hat{p}\hat{q}}$ , recovering GRPO. In the population limit ( $G \rightarrow \infty$ ),  $R_k \rightarrow 1 - q^k$  and  $Q'_{k-1} \rightarrow q^{k-1}$ , giving  $A_i \rightarrow q^{k-1}(r_i - p) / \sigma_k$  and  $m_S = m_F = p \sqrt{q^k / (1 - q^k)}$ .

**Remark.** If one were to naively set the baseline to  $R_k$  instead of  $\hat{p}$ , i.e.  $A_i = (r_i - R_k) / \sigma_k$ , one would obtain  $m_S = p(1 - R_k) / \sigma_k \neq m_F = q R_k / \sigma_k$  for  $k > 1$ . The per-sample baseline must remain at  $\hat{p}$  for sign symmetry to hold.

#### A.4.3 Mix Pass@1/Pass@ $k$ (Chen et al.)

Chen et al. (2025) also propose a convex combination of pass@1 and pass@ $k$  advantages:

$$A_i^{mix} = p \cdot \hat{A}_{pass@k} + q \cdot \hat{A}_{pass@1}.$$

Both components have the mean-centered structure  $C \cdot (r_i - p)$ :

$$\hat{A}_{pass@1} = \frac{r_i - p}{\sigma_1}, \quad \hat{A}_{pass@k} = \frac{q^{k-1}(r_i - p)}{\sigma_k}.$$

A linear combination of mean-centered terms remains mean-centered:

$$A_i^{mix} = \left( \frac{pq^{k-1}}{\sigma_k} + \frac{q}{\sigma_1} \right) (r_i - p) =: C_{mix}(r_i - p).$$

Since this is of the form  $C \cdot (r_i - p)$ , it is automatically sign-balanced. Following the GRPO pattern:

$$\nabla = C_{mix} \left[ q \sum_{i \in S} \nabla \log \pi_\theta(\tau_i) - p \sum_{i \in F} \nabla \log \pi_\theta(\tau_i) \right] = C_{mix} \cdot Bpq [\mathbf{m}_S - \mathbf{m}_F].$$

So  $m_S = m_F = C_{mix} \cdot pq$ . Noting that the success-side advantages are  $\hat{A}_s^{(k)} = C_k q = q^k / \sigma_k$  and  $\hat{A}_s^{(1)} = q / \sigma_1$ :

$$C_{mix} \cdot pq = p \left( p \cdot \underbrace{C_k q}_{\hat{A}_s^{(k)}} + q \cdot \underbrace{C_1 q}_{\hat{A}_s^{(1)}} \right) = p \left( p \hat{A}_{pass@k} + q \hat{A}_{pass@1} \right),$$

confirming  $m_S = m_F = p \left( p \hat{A}_{pass@k} + q \hat{A}_{pass@1} \right)$ .

## A.5 Biasing towards Negatives with a Shifted Baseline

A series of policy weights propose to shift up or down the positive weights by adding a fixed offset to GRPO (Arnal et al., 2026) or to REINFORCE (Sutton, 1988), or using the minimum reward over the batch as an offset (Garg and Venkatesh, 2025). We’ll derive the advantage weight of AsymRL which can be generalized to other types of offsets, the advantage of AsymRL is:

$$A_i = r_i - (\bar{r} + \delta).$$

With binary rewards  $r_i \in \{0, 1\}$  and  $\bar{r} = p$ , the per-trajectory weights are:

$$A_s = 1 - p - \delta = q - \delta, \quad A_f = -p - \delta = -(p + \delta).$$

Splitting the gradient over successful and failed trajectories:

$$\begin{aligned} \nabla_{\text{AsymRL}} &= \sum_{i \in S} (q - \delta) \nabla \log \pi_\theta(\tau_i) - \sum_{i \in F} (p + \delta) \nabla \log \pi_\theta(\tau_i) \\ &= (q - \delta) \cdot |S| \cdot \mathbf{m}_S - (p + \delta) \cdot |F| \cdot \mathbf{m}_F \\ &= Bp(q - \delta) \mathbf{m}_S - Bq(p + \delta) \mathbf{m}_F, \end{aligned}$$

At  $\delta = 0$  we recover mean GRPO but in practice, Arnal et al. (2026) recommend  $\delta = 0.01$ .

## A.6 Quantile Baseline and MC-GRPO

The quantile baseline (Dabney et al., 2018) replaces the mean baseline with the  $\tau$ -quantile of the batch rewards:  $A_i = r_i - Q_\tau(\mathbf{r})$ , where  $Q_\tau$  is the  $\tau$ -th quantile. With binary rewards  $r_i \in \{0, 1\}$ , the quantile is a step function of the solve rate:

$$Q_\tau(\mathbf{r}) = \begin{cases} 0 & \text{if } p \leq \tau, \\ 1 & \text{if } p > \tau. \end{cases}$$

*Case 1:  $p \leq \tau$  (hard problems).* The baseline is 0, so  $A_s = 1$ ,  $A_f = 0$ . Only successes contribute:

$$\nabla = \sum_{i \in S} \nabla \log \pi_\theta(\tau_i) = Bp \bar{\nabla}_S.$$

Hence  $m_S = p$  and  $m_F = 0$ .

Case 2:  $p > \tau$  (easy problems). The baseline is 1, so  $A_s = 0$ ,  $A_f = -1$ . Only failures contribute:

$$\nabla = - \sum_{i \in F} \nabla \log \pi_{\theta}(\tau_i) = -Bq \bar{\nabla}_F.$$

Hence  $m_S = 0$  and  $m_F = q$ .

Combining both cases:  $m_S = p \mathbf{1}[p \leq \tau]$  and  $m_F = q \mathbf{1}[p > \tau]$ . The quantile baseline is always sign-biased for binary rewards: it learns only from successes on hard problems and only from failures on easy ones, never both simultaneously.

MC-GRPO (Kim, 2026) uses the median as the baseline,  $A_i = r_i - \text{med}(\mathbf{r})$ , which is the special case  $\tau = \frac{1}{2}$ . With binary rewards,  $\text{med}(\mathbf{r}) = \mathbf{1}[p > \frac{1}{2}]$ , so the masses reduce to  $m_S = p \mathbf{1}[p \leq \frac{1}{2}]$  and  $m_F = q \mathbf{1}[p > \frac{1}{2}]$ : the method switches abruptly from pure positive reinforcement to pure negative reinforcement at  $p = \frac{1}{2}$ .

## A.7 Binary Contrastive

The binary contrastive weight (Greensmith et al., 2004) is  $W(\tau) = \mathbf{1}_{r=1} - \frac{\bar{p}}{1-\bar{p}} \mathbf{1}_{r=0}$  so we have  $m_S = p \times 1$  and  $m_F = (1-p) \times \frac{p}{1-p} = p$ .

## A.8 Power Norm

The Power Norm advantage (Andrychowicz et al., 2021) is  $A_i = \frac{r_i - \bar{r}}{[\bar{r}(1-\bar{r})]^\gamma}$ . With binary rewards and  $\bar{r} = p$ :

$$A_s = \frac{q}{(pq)^\gamma}, \quad A_f = \frac{p}{(pq)^\gamma}.$$

The gradient is:

$$\nabla = \frac{q}{(pq)^\gamma} \cdot Bp \mathbf{m}_S - \frac{p}{(pq)^\gamma} \cdot Bq \mathbf{m}_F = \frac{Bpq}{(pq)^\gamma} [\mathbf{m}_S - \mathbf{m}_F].$$

Hence  $m_S = m_F = pq/(pq)^\gamma = p^{1-\gamma}q^{1-\gamma}$ . At  $\gamma = 1/2$  this recovers GRPO; at  $\gamma = 0$  it recovers Dr. GRPO.

## A.9 Function-Based Policy Weights

Both Softmax and Logmeanexp aggregate rewards through the exponential partition function. With  $|S| = Gp$  successes and  $|F| = Gq$  failures in a batch of  $G$  rollouts, the partition function is:

$$Z := |S| e^\beta + |F| = G(pe^\beta + q) = G[1 + p(e^\beta - 1)].$$

The per-sample softmax weights are  $\text{softmax}_\beta(1) = e^\beta/Z$  and  $\text{softmax}_\beta(0) = 1/Z$ .

Softmax (Shao et al., 2024). The advantage  $A_i = \text{softmax}_\beta(r_i) - 1/G$  subtracts a uniform baseline. Substituting:

$$A_s = \frac{e^\beta}{Z} - \frac{1}{G} = \frac{(e^\beta - 1)q}{Z}, \quad A_f = \frac{1}{Z} - \frac{1}{G} = \frac{-p(e^\beta - 1)}{Z}.$$

The gradient is:

$$\nabla = A_s \cdot Gp \mathbf{m}_S - |A_f| \cdot Gq \mathbf{m}_F = \frac{(e^\beta - 1)pq}{pe^\beta + q} [\mathbf{m}_S - \mathbf{m}_F].$$

Hence  $m_S = m_F = \frac{(e^\beta - 1)pq}{1 + p(e^\beta - 1)}$ , which is sign-balanced. As  $\beta \rightarrow 0$ , this recovers Dr. GRPO; as  $\beta \rightarrow \infty$ , it converges to the pass@k advantage.

*Logmeanexp* (Jiang et al., 2025). The advantage  $A_i = \text{lme}_\beta(\mathbf{r}) - \text{lme}_\beta(\mathbf{r}_{-i})$  uses the same partition function through a leave-one-out log-difference, where  $\text{lme}_\beta(\mathbf{r}) = \frac{1}{\beta} \log(Z/G)$ . Removing a success shifts  $Z \rightarrow Z - e^\beta$  while removing a failure shifts  $Z \rightarrow Z - 1$ . Taking the log breaks the sign symmetry: removing a high-weight success changes  $\log Z$  more than removing a failure. In expectation:

$$m_S = \frac{pe^\beta}{pe^\beta + q}, \quad m_F = \frac{q}{pe^\beta + q}.$$

The ratio  $m_S/m_F = pe^\beta/q$  is sign-biased: successes are exponentially upweighted. As  $\beta \rightarrow 0$ ,  $m_S \rightarrow p$  and  $m_F \rightarrow q$  (REINFORCE). As  $\beta \rightarrow \infty$ ,  $m_S \rightarrow 1$  and  $m_F \rightarrow 0$  (pure positive reinforcement).

## A.10 HA-DW

HA-DW (Yang et al., 2026) uses a hardness-aware dynamic weight:  $W(\tau) = A \cdot \lambda \exp(-\text{sgn}(\hat{A}) \text{sgn}(\hat{r} - C_t) |\hat{r} - C_t|)$ , where  $C_t$  is a running baseline. With binary rewards, letting  $A$  denote the base advantage and the exponential modulate based on whether the reward exceeds the baseline:

$$m_S = f(C_t, p) qp, \quad m_F = qp,$$

where  $f(C_t, p)$  depends on the exponential modulation. The negative mass matches Dr. GRPO while the positive mass is scaled by a hardness-dependent factor.

## A.11 ReLU Advantage

The ReLU advantage (Srinivasan et al., 2018) is  $A_i = \max(0, r_i - \bar{r})$ . With binary rewards:  $A_s = \max(0, q) = q$ ,  $A_f = \max(0, -p) = 0$ . gives a purely positive gradient:  $\nabla = q \cdot Bp \mathbf{m}_S = Bpq \mathbf{m}_S$ . Hence  $m_S = pq$  and  $m_F = 0$ . ReLU is sign-biased: it reinforces successes with the same magnitude as Dr. GRPO but completely ignores failures.

# B Extension to Multi-Turn and Connection to Resampling

## B.1 Generalizing the framework to multi-turn rollouts

The decomposition  $\nabla_\theta J = m_S \bar{\nabla}_S - m_F \bar{\nabla}_F$  relies only on linearity of expectation over per-token weights and is therefore agnostic to whether a trajectory is generated in a single turn or interleaved with environment / tool feedback across multiple turns. We make the extension explicit here.

*Setup.* A multi-turn rollout decomposes a trajectory as  $\tau = (\tau_1, \tau_2, \dots, \tau_T)$ , where turn  $t$  is generated from a state  $s_t$  that depends on  $(\tau_1, \dots, \tau_{t-1})$  and any intervening environment observations  $o_{<t}$ . Tokens generated by the policy carry a per-token weight  $w_t$ ; environment-supplied tokens are masked from the gradient. The policy gradient is:

$$\nabla_\theta J = \mathbb{E}_\tau \left[ \sum_{t=1}^T \sum_{a \in \tau_t} w_{t,a} \nabla_\theta \log \pi_\theta(a | s_t) \right]. \quad (15)$$

Splitting  $w_{t,a} = w_{t,a}^+ - w_{t,a}^-$  and summing over turns yields

$$\nabla_\theta J = \sum_{t=1}^T [m_S^{(t)} \bar{\nabla}_S^{(t)} - m_F^{(t)} \bar{\nabla}_F^{(t)}], \quad (16)$$

with per-turn masses

$$\begin{aligned} m_S^{(t)} &= \rho_t \cdot \mathbb{E}[w_t^+ | \text{turn } t \text{ reached}], \\ m_F^{(t)} &= \rho_t \cdot \mathbb{E}[w_t^- | \text{turn } t \text{ reached}], \end{aligned}$$

where  $\rho_t := \Pr_{\pi_\theta}(\text{turn } t \text{ is reached})$  is the *reachability factor* of turn  $t$ . Single-turn is the special case  $T = 1$ ,  $\rho_1 = 1$ , recovering Section 2 exactly.

---

**Algorithm 1** Power  $\alpha$  (static)

---

**Require:** Policy  $\pi_\theta$ , prompts  $\mathcal{Q}$ , unit tests  $\mathcal{T}_q$ , power  $\alpha \geq 1$

- 1: **for** step  $t = 1, \dots, T$  **do**
- 2:   Sample  $G$  rollouts per prompt; score  $r_i \leftarrow \text{EXEC}(\tau_i, \mathcal{T}_q)$
- 3:    $\bar{r} \leftarrow \frac{1}{|\mathcal{B}|} \sum_i r_i$
- 4:   **for** each rollout  $i \in \mathcal{B}$  **do**
- 5:      $A_i \leftarrow (1 - \bar{r})^{\alpha-1} (r_i - \bar{r})$
- 6:   **end for**
- 7:   Update  $\theta$  via PPO clipping ( $\varepsilon=0.2$ ) using advantages  $\{A_i\}$
- 8: **end for**

---

## B.2 Resampling failures with fixed context $\equiv$ Power $\alpha = 2$

A natural multi-turn schedule is to retry only failed prompts. We show that when the retry uses the same prompt context (no information added between attempts), one round of GRPO-on-failures produces an update with the same gradient mass as Power  $\alpha = 2$  (Table 1).

*Setup.* Fix a prompt with success rate  $p$  and let  $q := 1 - p$ . Round 1 samples a batch of  $B$  rollouts and applies GRPO. Round 2 only fires for prompts that failed in round 1 (probability  $q$ ); it samples a fresh batch of  $B$  rollouts from the same prompt context and applies GRPO again.

For round 1 mass we have the standard GRPO  $m_S^{(1)} = m_F^{(1)} = Bpq$ . The reachability factor for round 2 is  $\rho_2 = q$ . Because the resample shares the same context, the within-round success rate is again  $p$  and within-round GRPO yields the same closed form  $Bpq$ . Multiplying by reachability:  $m_S^{(2)} = m_F^{(2)} = \rho_2 \cdot Bpq = q \cdot Bpq = Bpq^2$ .

*Interpretation.* The  $q^{\alpha-1}$  multiplier in the Power- $\alpha$  family is therefore not arbitrary: for integer  $\alpha$ , it is exactly the marginal contribution of one extra GRPO retry on the failed prompts. It can be implemented either as a within-batch reweighting (cheap, no extra rollouts) or as an explicit resample loop.

## C FADE Scheduler Additional Results

Algorithm 2 details the full FADE procedure. Two exponential moving averages track the online solve rate  $\hat{p}$  and policy entropy  $\hat{H}$ , which respectively control the difficulty focus  $\alpha$  and the sign bias  $\delta$ . Crucially,  $\alpha$  and  $\delta$  are updated from the smoothed EMAs, while the per-sample advantage uses the batch-level mean  $\bar{r}$ . For binary rewards, the resulting per-prompt gradient masses are  $m_S = pq^\alpha$  and  $m_F = pq^\alpha/\delta$ , so the sign ratio is  $m_S/m_F = \delta$ : when entropy exceeds  $H^*$ ,  $\delta = 1$  (sign-balanced); as entropy drops,  $\delta$  decreases and the negative mass dominates, triggering exploitation.

Figure 9 summarizes our ablation study on each FADE component.

$$\begin{aligned} \delta(t) &= \delta_0 - (\delta_0 - \delta_{\min}) \frac{\log(1 + t/\tau_\delta)}{\log(1 + T/\tau_\delta)}, \\ \delta_0 &= 1.0, \quad \delta_{\min} = 0.802, \quad \tau_\delta = 12264, \end{aligned} \tag{17}$$

$$\begin{aligned} \alpha(t) &= \alpha_0 - (\alpha_0 - \alpha_{\min}) \frac{\log(1 + t/\tau_\alpha)}{\log(1 + T/\tau_\alpha)}, \\ \alpha_0 &= 2.0, \quad \alpha_{\min} = 1.917, \quad \tau_\alpha = 8500, \end{aligned} \tag{18}$$

where  $T$  is the total number of training steps. We fitted a logarithmic decay curve to the Qwen 2.5 7B results  $\alpha, \delta$  evolution per timestep to estimate these parameters.

---

**Algorithm 2** FADE: Focal Advantage with Dynamic Entropy (additions over Alg. 1)

---

**Require:** Policy  $\pi_\theta$ , prompts  $\mathcal{Q}$ , unit tests  $\mathcal{T}_q$ , target entropy  $H^*$ , max power  $\alpha_{\max}$ , EMA coefficient  $\beta=0.02$

- 1: Initialize  $\hat{p} \leftarrow 0.5$ ,  $\hat{H} \leftarrow H_0(\pi_\theta)$
  - 2: **for** step  $t = 1, \dots, T$  **do**
  - 3:   Sample  $G$  rollouts per prompt; score  $r_i \leftarrow \text{EXEC}(\tau_i, \mathcal{T}_q)$
  - 4:    $\bar{r} \leftarrow \frac{1}{|\mathcal{B}|} \sum_i r_i$ ,  $H_t \leftarrow \frac{1}{|\mathcal{B}|} \sum_i \frac{1}{T_i} \sum_t -\log \pi_\theta(a_t^{(i)} | q, a_{<t}^{(i)})$
  - 5:    $\hat{p} \leftarrow \beta \hat{p} + (1-\beta) \bar{r}$ ,  $\hat{H} \leftarrow \beta \hat{H} + (1-\beta) H_t$
  - 6:    $\alpha \leftarrow \text{clip}(\frac{3(1-\hat{p})}{2\hat{p}}, 1, \alpha_{\max})$ ,  $\delta \leftarrow \text{clip}(1 + \hat{H} - H^*, 0.3, 1)$
  - 7:   **for** each rollout  $i \in \mathcal{B}$  **do**
  - 8:      $A_i \leftarrow (1-\bar{r})^{\alpha-1} (r_i - \bar{r}) / \begin{cases} 1 & r_i \geq \bar{r} \\ \delta & r_i < \bar{r} \end{cases}$
  - 9:   **end for**
  - 10:   Update  $\theta$  via PPO clipping ( $\varepsilon=0.2$ ) using advantages  $\{A_i\}$
  - 11: **end for**
- 

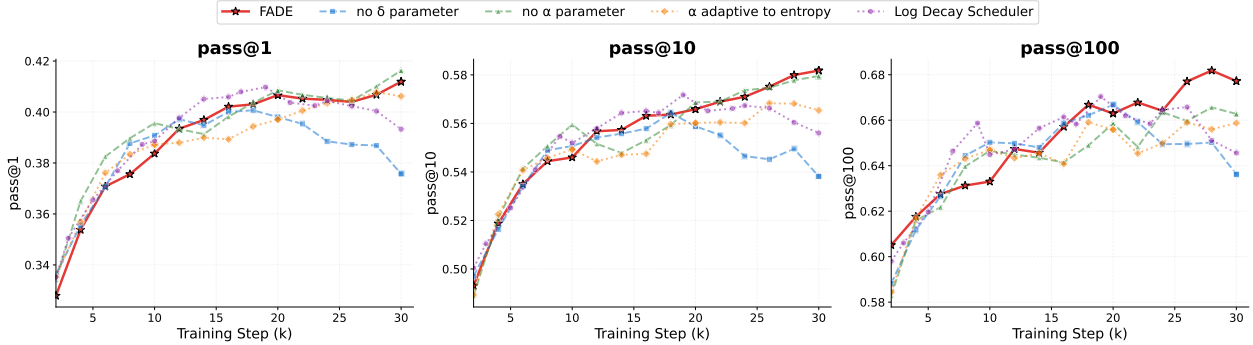


**Figure 9 Ablation Study on FADE** reveals adaptive  $\alpha$  only collapses whereas scheduling both on entropy and ablation  $\alpha$  worsens pass@100 diversity with Qwen 2.5 7B on LiveCodeBench at 8k reasoning.

## D Training and Evaluation Details

### D.1 Infrastructure and Hyperparameters

Similar to Gehring et al. (2025); Noukhovitch et al. (2025), we use an asynchronous distributed RL framework and a separate CPU cluster for code evaluations. Concretely we have a set of GPUs and CPUs that are divided into:

- samplers (H-100): produce code generations and send them to the CPUs,
- evaluators (CPU): evaluate the generated code against unit tests,
- trainers (H-100): receive the code tokens, their log probabilities and rewards to perform a backward update on our model.

The model travels between samplers and trainers so we always have the most updated model for generations. In practice, sampling is much slower than training so we have a trainer/sampler ratio of roughly 0.14 for Qwen 2.5 7B and 0.375 for CWM 32B. For Qwen 2.5 7B runs, we use 8 nodes (64 GPUs) with 1 trainer node and 7 sampler nodes. For CWM 32B runs, we use 32 nodes with 12 trainer nodes and 20 sampler nodes. Since we train with reasoning, we have varying sequence length and batch our answers by tokens rather than per sample using max tokens per batch = 32768. Since we generate maximum 8192 tokens for the Qwen 2.5

7B and 32768 for the CWM 32B, we have respectively at least 4 and 1 sample per batch.

**Table 2** Qwen 2.5 7B: gradient ratio vs. baseline and learning rate required to equalize gradient magnitude across normalization schemes (baseline LR =  $1e-7$ ).

Run / Normalization	Grad Ratio vs Baseline	LR to Equalize
pass_at_(8)	0.04x	2.67e-06
logmeanexp(0.4)	0.07x	1.52e-06
power_alpha(3)	0.20x	5.03e-07
power_alpha(2)	0.27x	3.67e-07
implicit_pass_at(8)	0.61x	1.63e-07
implicit_pass_at(2)	0.66x	1.51e-07
AsymRL	0.97x	$\sim 1e-7$
GRPO mean	<b>1.00x</b>	<b>1e-7</b>
MaxRL	2.82x	3.54e-08

We use all advantages within the PPO clipping framework

$$r_t(\theta) = \frac{\pi_\theta(a_t | s_t)}{\pi_{\theta_{\text{old}}}(a_t | s_t)}, \quad (19)$$

$$L_t(\theta) = -\min\left(r_t(\theta) \hat{A}_i, \text{clip}(r_t(\theta), 1-\varepsilon_{\text{low}}, 1+\varepsilon_{\text{high}}) \hat{A}_i\right) \quad (20)$$

with  $\varepsilon_{\text{low}} = \varepsilon_{\text{high}} = 0.2$  for Qwen 2.5 7B and  $\varepsilon_{\text{low}} = 0.2$ ,  $\varepsilon_{\text{high}} = 0.25$  for CWM 32B. The aggregated loss is  $\mathcal{L}(\theta) = \frac{1}{T_{\text{max}}} \sum_i \sum_{t \in \mathcal{A}_i} L_t(\theta)$  where  $\mathcal{A}_i$  is the set of agent (model-generated) token positions in rollout  $i$ , and  $T_{\text{max}}$  is the maximum token budget per microbatch ( $8192 \times \text{batch\_size}$  for the 7B model and  $32768 \times \text{batch\_size}$  for the 32B model).

## D.2 Full Evaluation Results

We evaluate models trained with different advantage functions at their peak performance during training (typically around  $20 \times 10^3$  RL steps), using the same training setup across all runs and varying only the reward normalization. To reduce variance across checkpoints, we select evaluation points where pass@ $k$  has stabilized, meaning at least 1000 consecutive steps yield similar results. For each advantage their required number of training steps can be found in table 6. For each pass@ $k$  metric, we draw  $2k$  samples and compute the mean over 400 groups of size  $2k$  to estimate the standard deviation. Results can be found for LiveCodeBench v6 in table 3, v5 in table 6 and for AIME benchmarks in table 4 and table 5.

## D.3 Gradient Ratios in Practice

In Section 4.1, we claim the speed of entropy collapse depends on the positive-to-negative ratio  $\rho(p) = \frac{m_S p}{m_F q}$  and show empirically in Figure 4 a strong correlation between this ratio and the final policy entropy after a fixed number of training steps. Mid-way through training (at approximately 15k gradient steps), we observed an average solve rate of 0.3 for Qwen 2.5 7B and 0.5 for the CWM 32B. Using those values for  $\bar{p}$ , Table 7 shows the positive to negative mass ratios used per policy weight. All sign-balanced methods share  $\rho(p) = \frac{p}{1-p}$  since  $m_S = m_F$ .

To compare entropy collapse under equalized gradient scales, we adapt the learning rate  $\eta$  for each method using their  $\eta \cdot \max_i |A_i|$  magnitude. The reference  $\eta$  is  $1e-7$  for the Qwen 2.5 7B and  $1.8e-7$  for CWM 32B (see table 2). Using GRPO as a reference, policy weights with smaller maximum values get larger learning rates and vice versa. This ensures differences are due to the policy weight function, not its overall scale. Figure 14 shows how non-equalized learning rate can speed up or slow down entropy collapse.

Method	Qwen 2.5 7B SFT			CWM 32B			
	8k budget			30k budget			
	p@1	p@10	p@100	p@1	p@10	p@100	p@200
<i>Baselines</i>							
SFT model	15.2	42.3	52.2	37.5±3.4	54.0±4.0	69.0	72.5
REINFORCE	29.4±0.0	45.3±5.2	55.8±3.0	—	—	—	—
GRPO	37.4±2.4	53.6±2.1	62.5±0.2	62.0±1.6	76.7±0.6	83.7	85.0
<i>Existing methods</i>							
Implicit p@2	39.7±1.7	56.2±0.8	65.2±0.9	—	—	—	—
Implicit p@8	38.0±2.0	54.3±1.6	64.7±0.6	—	—	—	—
LME $\beta = 0.4$	35.9±2.8	52.5±3.1	62.0±1.0	—	—	—	—
Pass@8	33.8±2.5	51.7±3.1	61.1±1.0	—	—	—	—
Asym. norm	38.1±1.7	53.4±1.0	63.0±0.6	—	—	—	—
<i>New Methods</i>							
Asym $\delta = 0.5$	35.7±2.0	51.8±1.4	60.5±0.1	—	—	—	—
Power $\alpha = 2$	40.3±1.2	56.6±0.7	66.0±0.9	61.2±1.4	76.7±0.6	82.9	83.9
Power $\alpha$ asym (2,2)	40.0±1.7	56.0±1.3	64.9±0.2	62.8±1.1	76.2±0.8	83.3	84.6
FADE $h^* = 1.0$	<b>40.7±1.0</b>	<b>58.0±0.7</b>	<b>68.2±1.2</b>	<b>63.1±1.2</b>	<b>77.9±0.9</b>	<b>85.3</b>	<b>86.3</b>

**Table 3** Pass@ $k$  evaluation results with standard deviations on LiveCodeBench v6 (454 problems, Aug 2024-May 2025).

## E Pass@ $k$ Scaling Law: Proof and Fitting Details

We frame diversity as: how fast does pass@ $k$  increase with  $k$ ? If we define  $\text{pass}@k = \mathbb{E}_p[1 - (1 - p)^k] = 1 - \mathbb{E}_p[(1 - p)^k]$  where  $p$  is the per-problem pass@1 rate, the asymptotic behavior depends on the distribution of  $p$  near 0.

### E.1 Theory of Scaling Laws of Pass@ $k$

We adapt the proof from Schaeffer et al. (2025). Let  $p_D(p)$  be the density of pass@1 rates over a dataset  $D$ , and  $\text{pass}_{D@k} = \mathbb{E}_{p \sim D}[1 - (1 - p)^k]$ .

**Theorem E.1** (Dichotomy of Scaling Behavior). *The asymptotic behavior of  $\text{pass}_{D@k}$  as  $k \rightarrow \infty$  is determined by  $p_D(p)$  near  $p = 0$ :*

- Power-law regime:** If  $p_D(p) = Cp^{b-1} + O(p^{b-1+\theta})$  as  $p \rightarrow 0^+$  ( $C, b, \theta > 0$ ), then  $\text{pass}_{D@k} = 1 - C\Gamma(b)k^{-b} + o(k^{-b})$ .
- Rapidly decaying regime:** If  $p_D(p) \leq C \exp(-c/p^\alpha)$  as  $p \rightarrow 0^+$  ( $c, \alpha > 0$ ), then  $1 - \text{pass}_{D@k} = o(k^{-b})$  for all  $b > 0$ .

*Proof.* Since  $(1 - p)^k \approx e^{-kp}$  for large  $k$ , we have  $1 - \text{pass}_{D@k} \approx \int_0^1 e^{-kp} p_D(p) dp$ , a Laplace-type integral dominated by small  $p$ .

**Case 1.** With  $p_D(p) \sim Cp^{b-1}$ , the tail  $[\epsilon, 1]$  is exponentially small in  $k$ , so  $1 - \text{pass}_{D@k} \approx C \int_0^\infty p^{b-1} e^{-kp} dp = Ck^{-b} \Gamma(b)$ , where the last step uses  $u = kp$ .

**Case 2.** The integrand  $e^{-kp-c/p^\alpha}$  is maximized at  $p^* \sim k^{-1/(1+\alpha)}$ , giving  $\int_0^1 e^{-kp} p_D(p) dp \leq \exp(-\Omega(k^{\alpha/(1+\alpha)}))$ , which decays faster than any power of  $k$ .  $\square$

### E.2 From Asymptotic to Empirical Fits

As shown above, the  $k$  vs. pass@ $k$  scaling law follows an exponential or polynomial growth as  $k \rightarrow \infty$  based on the distribution of solve rates near  $p$ . We analyze the distribution of per-prompt solve rates  $\hat{p}$  across the training set at fixed checkpoint steps for the Qwen 2.5 7B (Figures 10a) and CWM 32B models (Figure 10b). Rather than shifting smoothly from hard to easy, the solve-rate distribution is strongly bimodal at both

**Table 4** Pass@k evaluation on AIME benchmarks for Qwen 2.5 7B SFT (14k training budget) (%).

Method	AIME2024			AIME2025		
	p@1	p@10	p@100	p@1	p@10	p@100
<i>Baselines</i>						
SFT baseline	32.6 $\pm$ 4.2	65.3 $\pm$ 1.2	78.1 $\pm$ 4.2	21.3 $\pm$ 3.5	46.2 $\pm$ 3.0	70.8 $\pm$ 5.0
GRPO	37.9 $\pm$ 5.2	70.4 $\pm$ 1.9	81.4 $\pm$ 2.7	24.6 $\pm$ 3.2	50.3 $\pm$ 2.5	68.3 $\pm$ 3.3
<i>Existing methods</i>						
Implicit p@2	36.0 $\pm$ 4.2	66.1 $\pm$ 2.8	73.3 $\pm$ 0.0	24.9 $\pm$ 3.0	45.0 $\pm$ 3.3	63.7 $\pm$ 4.7
Implicit p@8	40.3 $\pm$ 4.0	69.6 $\pm$ 1.9	76.7 $\pm$ 1.7	27.5 $\pm$ 3.4	52.5 $\pm$ 3.3	69.1 $\pm$ 5.0
Asym. norm	40.2 $\pm$ 4.2	69.1 $\pm$ 1.7	78.3 $\pm$ 4.3	27.5 $\pm$ 3.4	52.0 $\pm$ 2.4	63.3 $\pm$ 3.3
Pass@8	35.7 $\pm$ 4.6	68.0 $\pm$ 2.9	82.1 $\pm$ 3.2	24.4 $\pm$ 3.0	49.3 $\pm$ 2.4	70.4 $\pm$ 6.9
LME $\beta = 0.4$	39.3 $\pm$ 4.7	71.0 $\pm$ 3.4	82.4 $\pm$ 1.9	25.4 $\pm$ 3.1	51.0 $\pm$ 4.0	<b>72.5 <math>\pm</math>6.9</b>
<i>New methods</i>						
Asym. GRPO $\delta = 0.5$	43.1 $\pm$ 4.6	69.1 $\pm$ 1.0	79.2 $\pm$ 2.7	26.6 $\pm$ 3.0	48.3 $\pm$ 3.2	66.0 $\pm$ 3.2
Power $\alpha = 2$	41.8 $\pm$ 4.4	70.4 $\pm$ 1.3	77.9 $\pm$ 1.7	26.6 $\pm$ 2.8	50.0 $\pm$ 3.0	64.9 $\pm$ 1.7
Power $\alpha$ asym (2,2)	41.1 $\pm$ 4.2	71.9 $\pm$ 1.9	<b>86.1 <math>\pm</math>5.0</b>	27.4 $\pm$ 3.4	53.3 $\pm$ 2.2	66.6 $\pm$ 2.7
<i>FADE (ours)</i>						
FADE $h^* = 0.5$	41.9 $\pm$ 4.2	70.9 $\pm$ 1.1	79.6 $\pm$ 3.2	27.8 $\pm$ 2.7	52.9 $\pm$ 2.2	67.5 $\pm$ 4.3
FADE $h^* = 1.0$	<b>44.5 <math>\pm</math>4.6</b>	<b>72.3 <math>\pm</math>2.2</b>	83.7 $\pm$ 5.0	28.6 $\pm$ 3.4	53.8 $\pm$ 1.8	68.3 $\pm$ 1.9
FADE $h^* = 1.3$	44.3 $\pm$ 3.6	71.8 $\pm$ 2.0	80.8 $\pm$ 0.0	<b>31.3 <math>\pm</math>3.7</b>	<b>55.4 <math>\pm</math>2.9</b>	70.7 $\pm$ 1.9

**Table 5** Pass@k evaluation on AIME benchmarks for CWM 32B (30k training budget) (%).

Method	AIME2024			AIME2025		
	p@1	p@10	p@100	p@1	p@10	p@100
<i>Baselines</i>						
GRPO	58.4 $\pm$ 5.0	87.4 $\pm$ 0.8	<b>94.9 <math>\pm</math>1.7</b>	46.1 $\pm$ 4.8	77.2 $\pm$ 2.0	80.0 $\pm$ 0.0
<i>New methods (ours)</i>						
Power $\alpha = 2$	41.2 $\pm$ 5.3	81.9 $\pm$ 2.6	91.7 $\pm$ 1.7	27.4 $\pm$ 4.6	70.4 $\pm$ 2.9	<b>84.6 <math>\pm</math>3.2</b>
Power asym (2,2)	<b>70.3 <math>\pm</math>3.5</b>	89.2 $\pm$ 1.5	93.3 $\pm$ 1.7	<b>58.7 <math>\pm</math>4.2</b>	78.1 $\pm$ 1.4	83.3 $\pm$ 3.2
Asym FADE $h^* = 1.0$	64.6 $\pm$ 4.7	<b>89.5 <math>\pm</math>2.6</b>	93.3	52.7 $\pm$ 5.1	<b>78.5 <math>\pm</math>1.6</b>	83.1

scales, with most mass concentrated near  $p = 0$  (unsolved) and  $p = 1$  (fully solved) and relatively little weight in the intermediate range.

We found both the power and exponential laws tended to overestimate pass@k values for lower  $k$  so for geometric fitting rather than asymptotic behavior prediction, we opted for a shifted power law. We use  $G(k) = \exp(-a(k + k_0)^{-b})$  with three parameters:  $a$  (scale),  $b$  (exponent), and  $k_0$  (horizontal shift) (see Figure 11, 12, 13) which in practice has the lowest MSE across problem difficulty splits.

## F Proof Entropy Change

We adapt the proof of Cui et al. (2025) to the discrete update setting and generalize to advantages with  $\mathbb{E}[A] \neq 0$ .

**Theorem F.1** (Entropy change per update step). *Let  $\pi_\theta(a|s)$  be a policy parameterized by  $\theta$ , with entropy  $\mathcal{H}(\pi) = -\sum_a \pi(a|s) \log \pi(a|s)$ . Suppose the parameters are updated via a policy gradient step  $\theta_{t+1} = \theta_t + \eta \mathbb{E}_{a \sim \pi}[A \nabla_\theta \log \pi_\theta(a|s)]$  where  $A$  is an advantage function with  $\mathbb{E}[A] = m_S - m_F$ . Then, under a local projection assumption, the per-step entropy change satisfies:  $\Delta \mathcal{H} \approx \eta [(m_S - m_F) \mathcal{H} - \text{Cov}(A, \log \pi_\theta)] + O(\eta^2)$ , where the approximation is a first-order Taylor expansion in the learning rate  $\eta$ .*

*Proof. Step 1: First-order approximation.* The entropy after one update is  $\mathcal{H}(\theta_{t+1}) = \mathcal{H}(\theta_t + \eta \mathbb{E}[A \nabla_\theta \log \pi])$ .

Method	Qwen 2.5 7B SFT				CWM 32B				
	8k budget				30k budget				
	Steps	p@1	p@10	p@100	Steps	p@1	p@10	p@100	p@200
<i>Baselines</i>									
SFT model	0	21.9±0.8	59.7±0.4	71.2±0.2	0	51.6±0.8	75.6±0.4	85.1	86.9
REINFORCE	17.5k	40.7±0.6	60.2±0.4	69.8±0.2	—	—	—	—	—
GRPO	20k	52.6±0.7	71.8±0.4	80.6±0.2	13.4k	77.3±0.6	89.0±0.2	92.0	92.6
<i>Existing methods</i>									
Implicit p@2	30k	55.3±0.7	73.3±0.4	80.9±0.2	—	—	—	—	—
Implicit p@8	30k	55.7±0.6	72.5±0.4	80.9±0.2	—	—	—	—	—
LME $\beta = 0.4$	20k	51.0±0.6	70.8±0.4	79.9±0.2	—	—	—	—	—
Pass@8	30k	48.3±0.7	70.5±0.4	80.0±0.2	—	—	—	—	—
Asym. norm	20k	54.1±0.6	70.9±0.4	79.2±0.2	—	—	—	—	—
<i>New Methods</i>									
Asym $\delta = 0.5$	40k	53.4±0.6	71.1±0.4	79.6±0.2	—	—	—	—	—
Power $\alpha = 2$	50k	<b>56.3±0.6</b>	<b>73.8±0.4</b>	<b>82.1±0.2</b>	17.5k	77.9±0.6	<b>89.4±0.2</b>	92.3	92.7
Power $\alpha$ asym (2,2)	20k	56.1±0.6	73.6±0.4	81.5±0.2	15k	78.7±0.5	88.9±0.2	92.0	92.6
FADE $h^* = 1.0$	30k	56.1±0.6	73.6±0.3	82.0±0.2	15k	<b>78.9±0.5</b>	89.3±0.2	<b>92.5</b>	<b>93.2</b>

**Table 6** Pass@ $k$  evaluation results with standard deviations on LiveCodeBench v5 (879 problems: 279 easy, 330 medium, 270 hard). 7B at 8k token budget, CWM 32B at 30k. Steps is the RL step selected for evaluation when evaluation results plateau (SFT = 0, i.e. no RL).

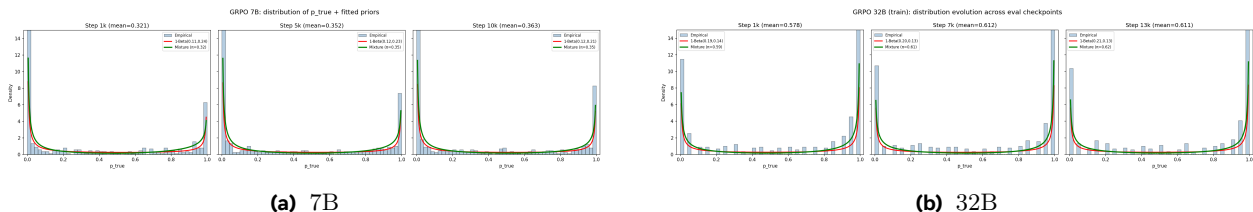


**Figure 10** Solve-rate distribution during training. Distribution of per-prompt solve rates at fixed checkpoint steps for (a) 7B and (b) 32B. We compare fits minimizing the mean squared error (MSE) with a Beta-Binomial distribution  $\text{BetaBin}(G, a, b)$  and a two component Beta mixture  $\pi, \text{Beta}(a_1, b_1) + (1 - \pi), \text{Beta}(a_2, b_2)$ .

Expanding to first order in  $\eta$ :

$$\Delta \mathcal{H} := \mathcal{H}(\theta_{t+1}) - \mathcal{H}(\theta_t) = \eta \nabla_{\theta} \mathcal{H}^{\top} \mathbb{E}[A \nabla_{\theta} \log \pi] + O(\eta^2). \quad (21)$$

This linearization is the source of the approximation: higher-order terms in  $\eta$  are neglected, so the result is accurate for small learning rates.

**Step 2: Entropy gradient.** Applying the product rule to  $\nabla_{\theta} \mathcal{H}$ :

$$\nabla_{\theta} \mathcal{H}(\pi) = - \sum_a (\nabla_{\theta} \pi(a|s) \log \pi(a|s) + \pi(a|s) \nabla_{\theta} \log \pi(a|s)). \quad (22)$$

Using the log-derivative trick  $\nabla_{\theta} \pi = \pi \nabla_{\theta} \log \pi$  and the identity  $\sum_a \pi(a|s) \nabla_{\theta} \log \pi(a|s) = \nabla_{\theta} \sum_a \pi(a|s) = 0$ , this simplifies to  $\nabla_{\theta} \mathcal{H}(\pi) = -\mathbb{E}_{a \sim \pi} [\log \pi \nabla_{\theta} \log \pi]$

**Step 3: Substitution.** Inserting (22) into (21):

$$\Delta \mathcal{H} \approx -\eta \mathbb{E}[\log \pi \nabla_{\theta} \log \pi]^{\top} \mathbb{E}[A \nabla_{\theta} \log \pi]. \quad (23)$$

**Step 4: Local projection assumption.** When the score vectors  $\nabla_{\theta} \log \pi$  span the relevant variation space, as holds exactly under natural policy gradients with the Fisher information metric, the inner product in parameter

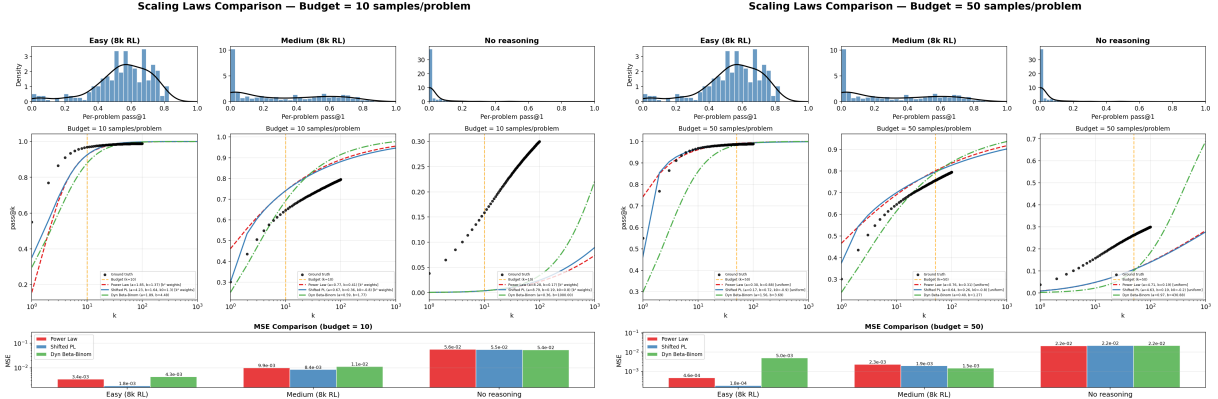


**Figure 11** Shifted power-law fits across budgets. Pass@ $k$  curves and their fitted shifted power laws at budget 10 (left) and budget 50 (right).

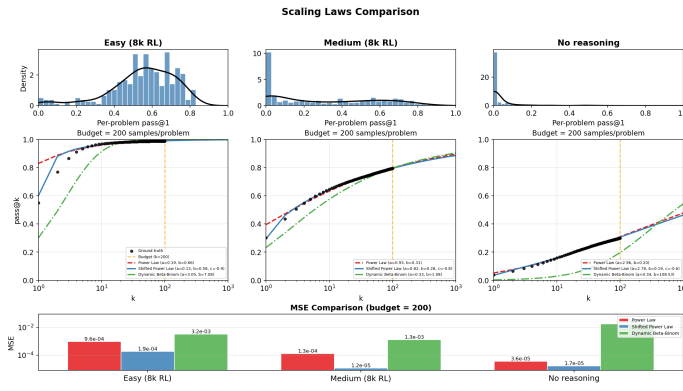


**Figure 12** Shifted Power Law Predicts Pass@ $k$  across different difficulty splits for an estimated pass@1 distribution (from 200 samples) with small (left), medium (middle) and high mass near 0.

Method	$\rho(p)$	$\rho(0.3)$	$\rho(0.5)$
<i>Sign-balanced (<math>m_S = m_F</math>)</i>			
All (GRPO, MaxRL, T2T, PA)	$\frac{p}{q}$	0.43	1.00
<i>Sign-biased (<math>m_S \neq m_F</math>)</i>			
REINFORCE	$\frac{p^2}{q^2}$	0.18	1.00
W-REINFORCE	$\frac{\lambda p^2}{q^2}$	$0.18\lambda$	$\lambda$
LogMeanExp ( $\beta = 0.4$ )	$\frac{p^2 e^\beta}{q^2}$	0.27	1.49
CoRPo ( $r_{\min} = 0.25$ )	$\frac{p^2(1-r_{\min})}{q^2 r_{\min}}$	0.55	3.00
Asym. GRPO $\delta = 0.5$	$\frac{\delta p}{q^2 r_{\min}}$	0.21	0.50
Asym. Power $\alpha (2,2)$	$\frac{p}{p^2 - \alpha_f} q^{\alpha_s - 2}$	1.00	1.00

**Table 7** Positive-to-negative ratio  $\rho(p) = \frac{m_S \cdot p}{m_F \cdot q}$  for each advantage function, evaluated at two training solve rates. Since Pass@ $k$  only has positive weights we remove it from the calculation.

space reduces to an expectation in action space:

$$\mathbb{E}[\log \pi \nabla_{\theta} \log \pi]^{\top} \mathbb{E}[A \nabla_{\theta} \log \pi] \approx \mathbb{E}[A \log \pi]. \quad (24)$$

This gives  $\Delta \mathcal{H} \approx -\eta \mathbb{E}[A \log \pi]$ .

**Step 5: Mean-covariance decomposition.** Decomposing  $\mathbb{E}[A \log \pi]$  using  $\mathbb{E}[A] = m_S - m_F$  and  $\mathbb{E}_{a \sim \pi}[\log \pi] = -\mathcal{H}$ :

$$\mathbb{E}[A \log \pi] = \mathbb{E}[A] \mathbb{E}[\log \pi] + \text{Cov}(A, \log \pi) = -(m_S - m_F) \mathcal{H} + \text{Cov}(A, \log \pi). \quad (25)$$

Substituting:

$$\Delta \mathcal{H} \approx \eta [(m_S - m_F) \mathcal{H} - \text{Cov}(A, \log \pi)]. \quad (26)$$

When  $m_S = m_F$  (sign-balanced advantages), the drift term vanishes and entropy dynamics are governed by the covariance alone:  $\Delta \mathcal{H} \approx -\eta \text{Cov}(A, \log \pi)$ .  $\square$

## G Weight-Estimation Variance of Power $\alpha$

The Power  $\alpha$  weight is  $w(p) = C p(1-p)^\alpha$ , where  $C$  normalizes the peak to match GRPO:

$$\max_p C p(1-p)^\alpha = \max_p p(1-p) = \frac{1}{4}. \quad (27)$$

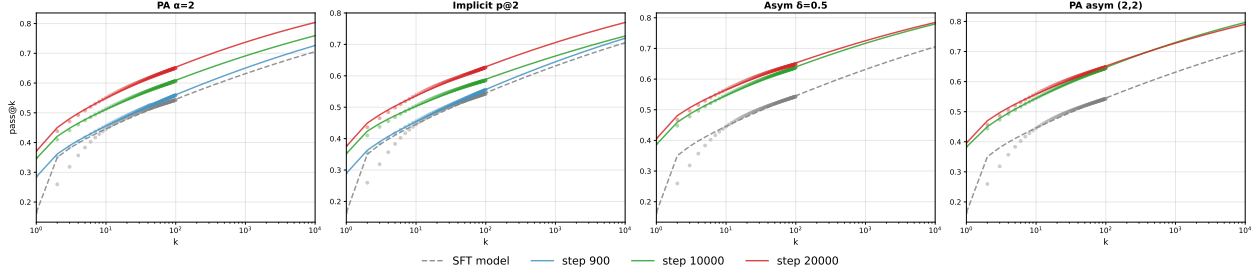


**Figure 13** Evolution of the  $k$  vs.  $\text{pass}@k$  curve during RL for different advantage functions with similar  $\text{pass}@100$  performances. We shorten the power  $\alpha$  series to PA.

The maximum of  $p(1-p)^\alpha$  is attained at  $p^* = 1/(1+\alpha)$ , giving  $C = \frac{(1+\alpha)^{1+\alpha}}{4\alpha^\alpha}$ .

In practice  $p$  is unknown; we estimate it from  $G$  independent rollouts as  $\hat{p} = k/G$ , where  $k \sim \text{Binomial}(G, p)$ , so  $\text{Var}(\hat{p}) = p(1-p)/G$ . Because the weight is a nonlinear function of  $\hat{p}$ , it inherits estimation noise. By the delta method ( $G$  reasonably large),

$$\text{Var}(w(\hat{p})) \approx [w'(p)]^2 \text{Var}(\hat{p}). \quad (28)$$

Differentiating  $w(p) = C p(1-p)^\alpha$ :

$$w'(p) = C(1-p)^{\alpha-1} [1 - (1+\alpha)p], \quad (29)$$

so the absolute variance is

$$\text{Var}(w(\hat{p})) = \frac{C^2 p(1-p)^{2\alpha-1} [1 - (1+\alpha)p]^2}{G}, \quad (30)$$

and the relative variance (coefficient of variation squared) is

$$\frac{\text{Var}(w)}{w^2} = \frac{[1 - (1+\alpha)p]^2}{G p(1-p)}. \quad (31)$$

This vanishes at the weight mode  $p = 1/(1+\alpha)$  and grows quadratically in  $\alpha$  away from it. Figure 7 shows the variance per solve rate  $p$  induced by different  $\alpha$  powers. Larger  $\alpha$  amplifies the weight-estimation noise for prompts away from the mode, adding a penalty  $\frac{\text{Var}(w)}{w^2}(s^2 + v)$  to the effective per-prompt noise (see Eq. (10)). This is a further downward force on the optimal  $\alpha$ , beyond the  $N_{\text{eff}}$  trade-off discussed in Section 4.3. The effect scales as  $O(1/G)$ .

At mean solve rate  $\bar{p}$ , replacing GRPO ( $\alpha=1$ ) with  $\alpha=3$  is justified only if harder prompts are more informative by  $s(p)/s(\bar{p}) \geq [2(1-p)]^2$ . Table 8 gives the concrete multipliers.

**Table 8** Minimum signal enrichment  $s(p)/s(0.5)$  required for  $\alpha=3$  to outperform GRPO at mean solve rate  $\bar{p}=0.5$  (iid noise,  $G=\infty$ ). At finite  $G$  the multipliers ease by  $\leq 30\%$  because the  $p=0.5$  reference is itself penalized away from  $\alpha=3$ 's weight mode at 0.25.

solve rate $p$	0.10	0.20	0.25	0.30	0.40
signal needed vs. GRPO	3.2×	2.6×	2.25×	2.0×	1.4×

## G.1 Sweet spot and the $\alpha$ - $p$ relationship

The most informative difficulty is where the per-prompt ratio peaks,  $\text{SNR}^2(p) = s(p)^2/v(p) \propto s(p)^2 p(1-p)$ . For  $s = e^{-cp}$ :

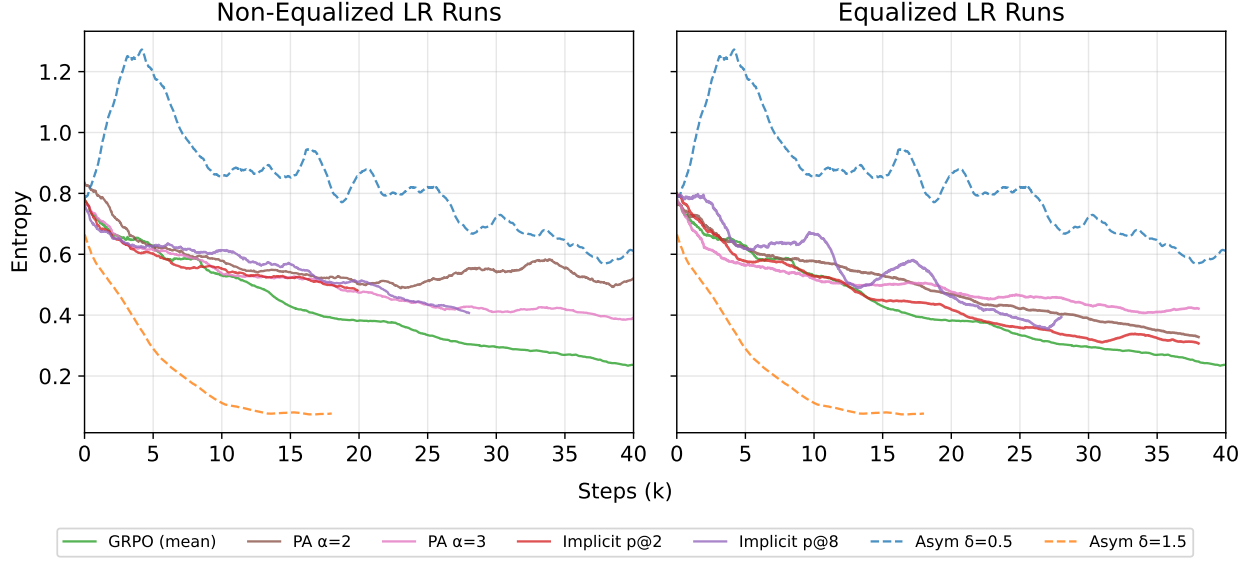


**Figure 14 Lower scale preserves entropy.** Different advantages at the same learning rate (right) vs. at equalized learning rates (left). Higher gradient ratios correlate with faster entropy collapse.

$s = e^{-cp}$	sweet spot $p^*$	$\alpha (G=\infty)$	$\alpha (G=16)$	$\alpha (G=8)$
$c = 0$ (flat)	0.50	1.00	0.90	0.92
$c = 0.5$ (mild)	0.38	1.20	1.06	1.06
$c = 1$ (moderate)	0.29	1.44	1.26	1.22
$c = 2$ (strong)	0.19	2.09	1.74	1.64

The flat case peaks at  $p = \frac{1}{2}$ ; a mild-to-moderate slope ( $c \approx 0.5-1$ ) moves the sweet spot into  $[0.3, 0.5]$ , with  $\alpha \approx 1.2-1.45$  for known weights falling to  $\approx 1.05-1.25$  once the weight-estimation correction is included ( $G=8-16$ ).

## H Weight-Space Analysis Details

### H.1 Rank-1 Collapse Theory

The per-token policy gradient with advantage  $A_i$  is  $g_i = A_i v_i \otimes h_i$ , where  $v_i = e_{y_i} - \pi_i \in \mathbb{R}^V$  and  $h_i \in \mathbb{R}^d$  is the hidden state. Decomposing  $h_i = \alpha_i u_1 + h_i^\perp$  along the top right singular vector  $u_1$  of  $G = \mathbb{E}[g_i]$  separates the batch gradient into a rank-1 signal and a higher-rank residual:

$$W_\Delta = \sum_{i=1}^N A_i v_i \otimes h_i = \underbrace{\left( \sum_{i=1}^N A_i \alpha_i v_i \right)}_{M_1 \text{ (rank 1)}} \otimes u_1 + \underbrace{\sum_{i=1}^N A_i v_i \otimes h_i^\perp}_{M_2 \text{ (higher rank)}}. \quad (32)$$

We quantify the degree of rank-1 collapse with  $r_1 = \sigma_1^2(W_\Delta) / \|W_\Delta\|_F^2$ , the fraction of the update’s Frobenius energy captured by its leading singular component:  $r_1 = 1$  means  $W_\Delta$  is exactly rank-1.

**Proposition H.1.** *Let  $\{(A_i, v_i, h_i)\}_{i=1}^N$  be i.i.d. with  $h_i = \alpha_i u_1 + h_i^\perp$ ,  $h_i^\perp \perp u_1$ ,  $u_1$  the top right singular vector of  $G$ ,  $\mathbb{E}[A_i^2 \|v_i\|^2 \|h_i\|^2] < \infty$ , and  $\mathbb{E}[A_i \alpha_i v_i] \neq 0$ . Then*

$$r_1 \xrightarrow{N \rightarrow \infty} \frac{\|\mathbb{E}[A_i \alpha_i v_i]\|^2}{\|\mathbb{E}[A_i \alpha_i v_i]\|^2 + \|R\|_F^2}, \quad (33)$$

where  $R = \mathbb{E}[A_i v_i \otimes h_i^\perp]$  is the higher-rank residual. In particular,  $r_1 \rightarrow 1$  iff  $R = 0$ .

**Table 9** Rank-1 dominance of the output head  $\Delta W$ . **(a)** At 500 steps, all methods are rank-1 dominant. **(b)** Over longer training, sign-biased methods maintain rank-1 while sign-balanced methods lose it; the effect weakens with model scale.

(a) 500 steps (7B)		(b) Converged					
Method	Rank-1%	Scale	Method	Sym	OH frac	$s_1/s_2$	Rank-1%
REINFORCE	95.4%	7B 8k	AsymGRPO( $\delta=0.3$ )	A	$\sim 97\%$	7.07	$\sim 78\%$
GRPO	91.4%	7B 16k	AsymGRPO( $\delta=0.5$ )	A	88.5%	6.96	96%
AsymGRPO	92.4%	7B 8k	REINFORCE	A	—	8.51	$\sim 81\%$
Power $\alpha=2$	83.9%	7B 8k	GRPO(mean)	S	$<10\%$	3.98	62%
		7B 8k	PA( $\alpha=2$ )	S	$<10\%$	3.61	61%
		14B	GRPO(mean)	S	3.2%	4.52	11%
		32B	AsymGRPO( $\delta=0.8$ )	A	3.96%	8.87	45.6%
		32B	GRPO(mean)	S	0.69%	2.24	2.2%

*Proof. Orthogonality.* Since  $h_i^\perp \perp u_1$  for all  $i$ , we have  $M_2 u_1 = \sum_i A_i v_i (h_i^{\perp \top} u_1) = 0$ . Therefore  $\langle M_1, M_2 \rangle_F = w^\top (M_2 u_1) = 0$ , giving  $\|W_\Delta\|_F^2 = \|M_1\|_F^2 + \|M_2\|_F^2$ .

*Signal.*  $M_1 = w \otimes u_1$  where  $w = \sum_i A_i \alpha_i v_i$ . Since  $u_1$  is a fixed (non-random) direction, the summands  $A_i \alpha_i v_i$  are i.i.d. with finite variance ( $\mathbb{E}[A_i^2 \alpha_i^2 \|v_i\|^2] \leq \mathbb{E}[A_i^2 \|v_i\|^2 \|h_i\|^2] < \infty$ ). By Kolmogorov’s strong law of large numbers,  $w/N \rightarrow \mathbb{E}[A_i \alpha_i v_i]$  a.s., so  $\|M_1\|_F^2/N^2 = \|w/N\|^2 \rightarrow \|\mathbb{E}[A_i \alpha_i v_i]\|^2$ .

*Residual.* Each entry of  $M_2/N = \frac{1}{N} \sum_i A_i v_i \otimes h_i^\perp$  converges a.s. to the corresponding entry of  $R = \mathbb{E}[A_i v_i \otimes h_i^\perp]$  by the same SLLN argument (finite variance is guaranteed by the second-moment condition). By continuity of  $\|\cdot\|_F$ ,  $\|M_2\|_F^2/N^2 \rightarrow \|R\|_F^2$  a.s.

*Combine.* By the SLLN,  $W_\Delta/N \rightarrow G$  entry-wise a.s. Since  $G u_1 = \mathbb{E}[A_i \alpha_i v_i]$  (the residual contributes nothing:  $R u_1 = 0$ ),  $u_1$  is the top right singular vector of  $G$  with singular value  $\sigma_1(G) = \|\mathbb{E}[A_i \alpha_i v_i]\|$ . By continuity of singular values (Weyl’s inequality:  $|\sigma_1(W_\Delta/N) - \sigma_1(G)| \leq \|W_\Delta/N - G\|_F \rightarrow 0$ ),  $\sigma_1(W_\Delta/N) \rightarrow \sigma_1(G)$ . Therefore  $r_1 = \sigma_1^2(W_\Delta/N)/\|W_\Delta/N\|_F^2 \rightarrow \sigma_1^2(G)/\|G\|_F^2$ , which equals Eq. (33) by the orthogonal decomposition  $\|G\|_F^2 = \|\mathbb{E}[A_i \alpha_i v_i]\|^2 + \|R\|_F^2$ .  $\square$

**Corollary H.2.** *Suppose failures arise from  $K$  independent reasoning modes with equal probability  $1/K$ , and let  $\mu_k = \mathbb{E}[h_i^\perp \mid \text{mode } k]$  denote the mean perpendicular hidden state of mode  $k$ . Split the residual by outcome:  $R = p R_S + \frac{q}{\delta} R_F$ . The failure residual decomposes as  $R_F = \frac{1}{K} \sum_{k=1}^K \mathbb{E}[A_i v_i \mid k] \otimes \mu_k$ . If the  $\mu_k$  are mutually orthogonal with  $\|\mu_k\| = \mu$  and  $\|\mathbb{E}[A_i v_i \mid k]\| = c$  for all  $k$ , then  $\|R_F\|_F^2 = c^2 \mu^2 / K$ , so  $\|R_F\| \sim 1/\sqrt{K}$ : more diverse failure modes yield a smaller residual. Setting  $\delta < 1$  amplifies the weight  $q/\delta$  on this shrinking  $R_F$  relative to the surviving  $R_S$  from correlated successes, accelerating the collapse  $r_1 \rightarrow 1$ .*

Table 9 highlights the rank 1 funnel effect.

We analyze how RL training with different advantage functions modifies the weights across three model scales:

- Qwen 2.5 7B:  $d=3584$ , 28 layers, 28 heads, 4 KV heads, vocab=152,064. 26 runs at 8k context, 8 runs at 16k.
- Qwen 2.5 14B:  $d=5120$ , 48 layers, 40 heads, 8 KV heads, vocab=152,064. 1 run (GRPO mean), 5 checkpoints.
- CWM 32B:  $d=6144$ , 64 layers, 48 heads, vocab=128,256. 6 runs.

*Analysis techniques.* For each run we compute  $\Delta = W_{\text{rl}} - W_{\text{sft}}$  and measure global  $L_2$  distance, per-layer  $L_2$  decomposition, pairwise cosine similarity of weight-change vectors with hierarchical clustering, full SVD of the output head delta, rank-1 decomposition  $\Delta \approx s_1 u v^\top$  with cross-run alignment of  $u/v$  vectors, and per-layer SVD across all weight matrices.

*Hidden-state analysis.* To measure the geometric structure of correct vs. failed trajectories, we extract the last-layer hidden states  $h_i \in \mathbb{R}^d$  for all tokens across a batch and project out the top right singular vector

$u_1$  of the batch gradient, yielding the perpendicular component  $h_i^\perp = h_i - (h_i^\top u_1)u_1$ . We then compute the mean pairwise cosine similarity  $\hat{\rho}$  of these  $h^\perp$  vectors separately for correct and failed trajectory groups. This measures how much hidden-state structure survives beyond the dominant rank-1 direction. We also compute group-conditional residual norms  $\|R_{\text{group}}\|_F = \|\frac{1}{N} \sum_{i \in \text{group}} v_i \otimes h_i^\perp\|_F$ , where  $v_i = e_{y_i} - \pi_i$  is the softmax error vector.<sup>1</sup>

The rank-1 left singular vector  $u \in \mathbb{R}^{|V|}$  of the output head delta reveals a universal ‘‘suppress non-code’’ direction shared across sign-biased runs: 99.93–99.97% of tokens have negative  $u$  values (Chinese, Russian, Thai, Arabic text; non-code identifiers),  $u$  is not sparse (50% of energy in  $\sim 22\%$  of vocab), and  $u$  vectors are nearly identical across sign-biased runs (cos = 0.93–0.99) and context lengths (cos = 0.82–0.96).

## H.2 Empirical Verification of Rank-1 Collapse

Correct trajectories are 3-4 $\times$  more correlated than failed ones in the perpendicular subspace, consistent across methods and training steps (Table 10).

**Table 10** Perpendicular correlation  $\hat{\rho}$  by trajectory outcome.

Method	Step	$\hat{\rho}_{\text{correct}}$	$\hat{\rho}_{\text{failed}}$	Ratio	$r_{\text{eff}}^\perp$ (C / F)
AsymGRPO	300	0.0177	0.0046	3.8 $\times$	614 / 727
AsymGRPO	3000	0.0193	0.0057	3.4 $\times$	644 / 765
AsymGRPO	10000	0.0157	0.0054	2.9 $\times$	674 / 797
AsymGRPO	15000	0.0126	0.0032	3.9 $\times$	699 / 824
GRPO	8000	0.0121	0.0050	2.4 $\times$	706 / 746
GRPO	60000	0.0294	0.0067	4.4 $\times$	913 / 948

*Residual norms and CLT baseline.* For each group  $g \in \{\text{success}, \text{failure}\}$  with  $N_g$  tokens, we compute the group-conditional residual  $R_g = \frac{1}{N_g} \sum_{i \in g} v_i \otimes h_i^\perp$ , where  $v_i = e_{y_i} - \pi_i$  and  $h_i^\perp$  is the hidden state with the top SVD direction projected out.

Under the null hypothesis that both groups have the same per-token covariance structure and differ only in sample size, each entry of  $R_g$  is an average of  $N_g$  i.i.d. terms with common variance  $\sigma^2$ . By the CLT,  $\|R_g\|_F^2 \approx Vd \cdot \sigma^2 / N_g$  (where  $V$  is the vocabulary size and  $d$  the hidden dimension), so the ratio of residual norms scales as  $\frac{\|R_F\|}{\|R_S\|} \approx \sqrt{\frac{N_S}{N_F}}$ . With  $N_S = 8,968$  and  $N_F = 54,700$  in our batches during the AsymGRPO  $\delta = 0.5$  training with Qwen 2.5 7B, this gives  $\sqrt{N_S / N_F} \approx 0.40$ . The measured ratio is  $\|R_F\| / \|R_S\| = 0.73$ – $0.79$  (Table 11), nearly twice the CLT prediction. This confirms that the gap is not an artifact of having more failure tokens: failures are genuinely more decorrelated in the perpendicular subspace, producing a smaller residual per token than successes do.

**Table 11** Group-conditional residual norms for the AsymGRPO  $\delta = 0.5$  run where  $S$ ,  $F$  are the set of correct and incorrect trajectories at a given timestep over a subset of samples from the training set.

Step	$\ R_S\ _F$	$\ R_F\ _F$	$\ R_F\  / \ R_S\ $	$ S  /  F $
3000	1.97	1.51	0.77	8,968 / 54,700
10000	2.00	1.46	0.73	8,968 / 54,700
15000	2.02	1.60	0.79	8,968 / 54,700

*Causal verification.* Since the rank-1 signal originates at the output head and propagates backward (Figure 5), Proposition H.1 predicts that asymmetric learning should be concentrated in the last few layers.

<sup>1</sup>These norms are unweighted by advantages ( $\mathbb{E}[v \otimes h^\perp \mid \text{group}]$  rather than  $\mathbb{E}[Av \otimes h^\perp \mid \text{group}]$ ), since advantages vary per-problem and across advantage functions. The projection direction is the top right singular vector of  $H$ , which may differ from  $u_1$  in Proposition H.1.

**Table 12** Cross-checkpoint direction alignment for a GRPO run (Qwen 2.5 7B, no-KL, 8k). Each entry is  $|\cos|$  between the leading singular vector of  $\Delta W = W_t - W_{\text{SFT}}$  at step  $t$  and at the final step (15,000). The output-head direction converges by step 1,200 ( $|\cos(u)| = 0.97$ ), while inner layers remain exploratory ( $|\cos(u)| < 0.25$ ) until step  $\sim 6,000$ , after which the model rescales the same directions with diminishing magnitude.

Step	Output head	Inner layers (mean $ \cos(u) $ )		
	$ \cos(u) $	L0–9	L10–19	L20–27
300	0.82	0.03	0.02	0.03
600	0.90	0.08	0.06	0.07
800	0.95	0.13	0.12	0.10
1,200	<b>0.97</b>	0.21	0.18	0.22
2,000	0.98	0.34	0.31	0.38
2,700	0.98	0.42	0.38	0.44
4,000	0.99	0.51	0.50	0.54
6,000	0.99	0.64	0.64	0.65
8,000	0.99	0.75	0.75	0.76
10,000	1.00	0.83	0.83	0.85
12,000	1.00	0.89	0.91	0.91
14,000	1.00	<b>0.97</b>	<b>0.97</b>	<b>0.97</b>

Periodically resetting the last 4 layers toward SFT weights erases most of AsymGRPO’s gains (with  $\delta = 0.5$ ), with pass@1 dropping back to the starting policy performance, while symmetric GRPO, with more distributed learning, benefits from the reset. This trade-off is scale-dependent: at 32B the rank-1 fraction drops from 78–96% to 45.6% for AsymGRPO (Table 9), and performance gaps between symmetric and asymmetric methods shrink accordingly (Tables 4 and 5).

**Corollary H.3** (Cross-step accumulation). *If at each optimization step  $t$  the batch gradient at the output head satisfies  $g_t \approx w_t \otimes u$  for a shared direction  $u \in \mathbb{R}^d$ , then the accumulated weight update  $W_\Delta = \sum_t \eta_t g_t \approx (\sum_t \eta_t w_t) \otimes u$  is exactly rank-1.*

The corollary gives a sufficient condition: if gradient directions align across steps, then rank-1 structure compounds. Empirically, cosine similarity between successive batch-gradient directions at the output head converges to  $|\cos| \approx 1.0$  from step  $\sim 600$  onward for asymmetric methods, confirming the condition during the exploitation phase. For symmetric methods the alignment remains lower, consistent with the higher effective rank of their accumulated updates.

### H.3 Alignment Dynamics in GRPO

Tracking a GRPO run at Qwen 2.5 7B across 16 checkpoints (step 300 to 15,000), cross-checkpoint direction alignment (Table 12) reveals a clear exploration-to-exploitation transition. The output head direction converges by step 1,200, while inner layers remain exploratory until step  $\sim 6,000$ . After that, the model scales up the same directions with diminishing magnitude. All values are  $|\cos|$  of the leading singular vector at each checkpoint’s  $W_\Delta = W_{\text{sft}} - W_{\text{rl}}$  versus the final (step 15,000) checkpoint:  $u$  (left/output-token direction) for the output head, and the layer-averaged  $|\cos(u)|$  for the transformer blocks grouped into early/mid/late thirds.